Missing sulfur in allotropes

Charlaganova, Liya

Missing Sulfur in Allotropes

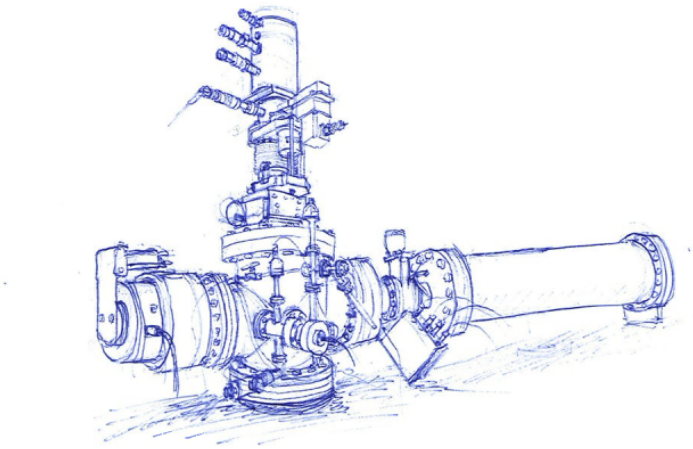

THESIS

submitted in partial fulfillment of the
requirements for the degree of

BACHELOR OF SCIENCE
in
ASTRONOMY

Author :	Liya Charlaganova
Student ID :	s2548852
Supervisor :	Dr. K. Chuang
2nd corrector :	Prof.dr.ir. T.H. Oosterkamp

Leiden, The Netherlands, June 22, 2023

Missing Sulfur in Allotropes

Liya Charlaganova

Leiden Observatory, Universiteit Leiden
P.O. Box 9500, 2300 RA Leiden, The Netherlands

June 22, 2023

Abstract

Sulfur is depleted in dense clouds by a factor of 100. It is speculated that sulfur is stored in UV-photoprocessed icy grains. For this bachelor research project, photochemistry of H_2S ice analogues in the lab was thoroughly studied. We grew pure H_2S ice samples and analyzed the UV irradiation kinetics as well as the resulting photoproducts using the CRYOPAD2 and MATRI^{2}CES setups at the Laboratory for Astrophysics at Leiden University. Irradiation and Temperature Programmed Desorption (TPD) experiments were performed on CRYOPAD2 yielding desorption temperatures for the first four hydrogenated sulfur chains (H_2S_x, x up to 4) and a photochemical desorption rate of 10^{-3} photons cm^{-2}. No evidence for the formation of pure sulfur allotropes was found. The MATRI^{2}CES setup, which is uniquely configured for laser ablated spectroscopy, allowed measurements of refractory photoproducts. The total sulfur budged in an irradiated H_2S ice has been found to be a factor 2.9 higher than the leftover unprocessed H_2S.

Chapter 1

Introduction

Sulfur is the tenth most common element in the universe and an essential component of cells. We have traced sulfur in its path from the interstellar medium (ISM) to minerals found on earth and measured sulfur abundance along the way. The story starts in the diffuse clouds of the ISM. In these low-density regions sulfur is mainly present in its gas-phase atomic form. Upper limits on atomic sulfur abundance are in agreement with the cosmic value. As the cloud shrinks and its density increases, atomic sulfur becomes depleted from the gas phase and no longer matches cosmic abundance by a factor of 100[1]. Larger sulfur bearing species also fail to account for this depletion[2]. This discrepancy was first observed at the end of the 20th century and has been dubbed the missing sulfur problem. Further cloud collapse leads to the formation of stars which continue accreting material from the surrounding protoplanetary disk. During this stage, the star is still relatively sulfur-poor compared to more developed stars with cosmic levels of sulfur abundance[3]. The missing sulfur is likely stored in sulfur minerals in trapped dust within the disk[4].
Water, one of the most abundant molecules in dense clouds, can form ice mantles on grain (dust) surfaces either through accretion or direct O and H chemistry on grain surfaces. This water-ice acts as a matrix for other species, keeping them in the ice mantle[5]. Composition of ice is dominated by water but contains simple molecules such as CO, CO_2, CH_3OH and NH_3 and trace sulfur bearing species[6]. So far three sulfur-bearing species have been identified in ice mantles: OCS, SO_2 and H_2S. Atomic sulfur is thought to accrete onto icy grains as CS and OCS, and subsequently react with H or O to form H_2S, SO_2 and OCS. H_2S, which is expected to be the most abundant sulfur species in interstellar ices, accounts for less than 25% of the sulfur budget[7]. SO_2 accounts for less than 6% of the budget[8] and OCS for less than 1%[9]. Comet ice can be measured more directly are thought to contain material from the interstel-

lar dense cloud. However, observations of the 67P/Churyumov-Gerasimenko comet by the *Rosetta* space probe show no significant sulfur depletion[10].
A possible reservoir of the missing sulfur in dense clouds is in UV-photoproducts formed as a result of far ultraviolet (FUV) background radiation. When a species absorbs a UV photon its energy may increase beyond its binding energy leading to sublimation from the ice (photodesorption). Furthermore, UV photons are energetic enough to break (dissociate) weaker chemical bonds leading to radical formation in the ice. This breaking of molecules is referred to as photodissociation. In the solid state radicals are reasonably close together allowing them to recombine in an exothermic reaction forming new products (photoconversion). If the binding energy of the product is low enough, it will escape (desorb) into the gas phase in a process referred to as photochemical desorption. When H_2S absorbs a UV photon it may dissociate into SH and H radical. These can then recombine in the following ways:

$$HS + H \rightarrow H_2S \tag{1.1}$$
$$HS + HS \rightarrow H_2S_2 \tag{1.2}$$

In the case of reaction 1.1, photochemical desorption is possible[11]. Newly formed products, such as H_2S_2 in reaction 1.2, will be referred to as photoproducts. This larger molecule can be disassociated further to form larger radicals which can in turn form larger molecules. Here we distinguish between two types of products: pure sulfur allotropes (S_x) and hydrogenated sulfur chains (H_2S_x). Both have been observed to form during irradiation of pure H_2S ice[12][7]. So far, products up to S_4 and H_2S_4 have been observed[12]. Larger products, which desorb above room temperature, have not been observed yet. These leftovers are referred to as refractory products. Models suggest that stable sulfur rings up to S_8 can form as well[13]. These sulfur rings are IR invisible due to the absence of a dipole moment, so we would not be able to detect them in space with vibrational spectroscopy spectra. This means that these large sulfur allotropes could be the missing sulfur reservoir.

The goal of this Bachelor Research Project is to further investigate the effects of UV irradiation of pure H_2S ice by experimentally simulating interstellar ices on two setups at the Laboratory for Astrophysics: CRYOPAD2 and MATRI^{2}CES. IR spectroscopy and mass spectroscopy are used to thoroughly study product formation and refractory products in the ices. The obtained rates for photodissociation and photochemical desorption of H_2S may help improve astrochemical ice grain models. Chapter 2 will describe the setups and discuss the experimental protocol. The experimental results are presented in Chapter 3 and discussed in Chapter 4 along with astronomical implications.

Chapter 2

Experimental

Experiments were performed on two cryogenic UHV (ultra-high vacuum) setups at the Laboratory for Astrophysics at Leiden University (CRYOPAD2 and MATRI^{2}CES, Figures 2.1 and 2.2, respectively). These two setups have similar capabilities in creating ices, but use different measurement methods. CRYOPAD2 uses fourier-transform infrared spectroscopy (FTIR) to measure the contents of the ice on the substrate and a quadrupole mass spectrometer (QMS) to measure the contents of the gasses present in the chamber. MATRI^{2}CES is fully customized to conduct mass spectrometry using time of flight mass spectrometer (TOF-MS) which is more sensitive than the QMS.
The main component of both setups is a cryogenic vacuum chamber which can go down to UHV conditions i.e. 10^{-11}mbar (CRYOPAD2) or 10^{-9} (MATRI^{2}CES). A closed-cycle helium cryostat is used to cool down a gold substrate on which the ice is grown. Both setups can cool down to temperatures of 15K and are able to warm the substrate up to 300K using a resisting heating unit attached to the substrate. A gas inlet coupled to the main chambers through a leak valve provides deposition rates close to 1 ML/min (monolayers per minute, 1 ML $= 10^{15}$ molecules cm^{-2}). A microwave-discharge hydrogen-flow lamp (MDHL) is equipped to the chamber through a UV-viewport and emits UV radiation. A shutter is positioned between the MDHL and the main chamber to control the irradiation steps.
Mass spectrometry is used to analyze the mass-to-charge ratio of molecules. In this project, the products of interest are neutral molecules so they must first be ionized in order to be detectable. An electron gun (usually set to 70eV) ionizes the gas phase contents by knocking of an electron from the molecule which produces a positively charged ion (cation). During ionization, the molecule can fall apart into smaller components and form ionic fragments which results in a mass spectrum for a single molecule species, also known as a fragmentation pattern.

In order to identify the molecule, the measured mass spectrum is compared to known fragmentation patterns of different molecules until a good match is found. The National Institute of Standards and Technology (NIST) Chemistry Webbook provides mass spectra for most common molecules which were ionized using 70eV electrons and is a good source of fragmentation patterns. For species not available, fragment pattern can be measured on the setup or borrowed from literature.
To get the ice components into the gas phase, CRYOPAD2 uses thermal desorption by heating up the substrate from 15 to 300K. Desorption temperature provides a way to identify the possible carrier of the desorption signals as these are species-dependent. MATRI^{2}CES uses laser ablation to induce instant and local thermal desorption of the ice: a short intense pulse hits a small part of the ice and heats it up to 600 K which instantly desorbs all material from the substrate and forms a gas plume. The gas plume is then analyzed using time-of-flight mass spectroscopy. This has two important consequences: first of all, the laser only ablates a small portion of the ice which means that multiple measurements can be performed on the same ice without the need to create the ice anew. Secondly, while CRYOPAD2 is only able to thermally desorb ices up to 300K, meaning that some molecules may still be in the ice at the end of the warm-up, the laser ablation technique can measure these refractory molecules as well. This greatly increases the capacities of MATRI^{2}CES, but it does make it a complex system. Since all ice is desorbed at once, it is much more difficult to distinguish the different molecules present in the ice due to fragmentation during ionization.

2.1 CRYOPAD2

This section will further describe the relevant workings and experimental methods of the CRYOPAD2 setup at the Laboratory for Astrophysics at Leiden University. For further technical details of the setup please refer to the latest PhD thesis of J. Terwisscha van Scheltinga[14] who provides the most recent description of the setup.

2.1.1 Fourier-Transform Infrared spectroscopy

CRYOPAD2 uses an Excalibur Series Fourier-Trasnform Infrared (FTIR) spectrometer set up in Reflective Absorbance Infrared Spectroscopy (RAIRS) mode to measure the vibrational absorption spectrum of the ice using a mercury cadmium telluride (MCT) detector. The different vibrational modes of molecules present in the ice absorb certain characteristic frequencies of light which results

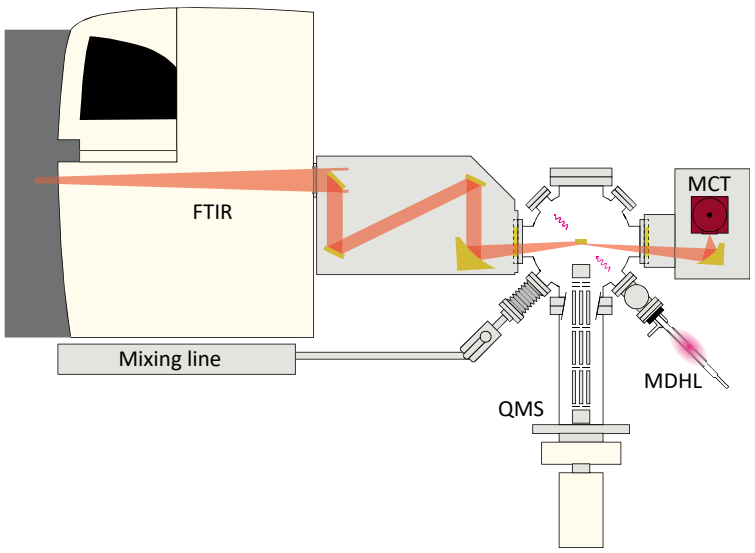

Figure 2.1: *Schematic top-down view of the CRYOPAD2 setup. Adapted from the PhD thesis of J. Terwisscha van Scheltinga[14].*

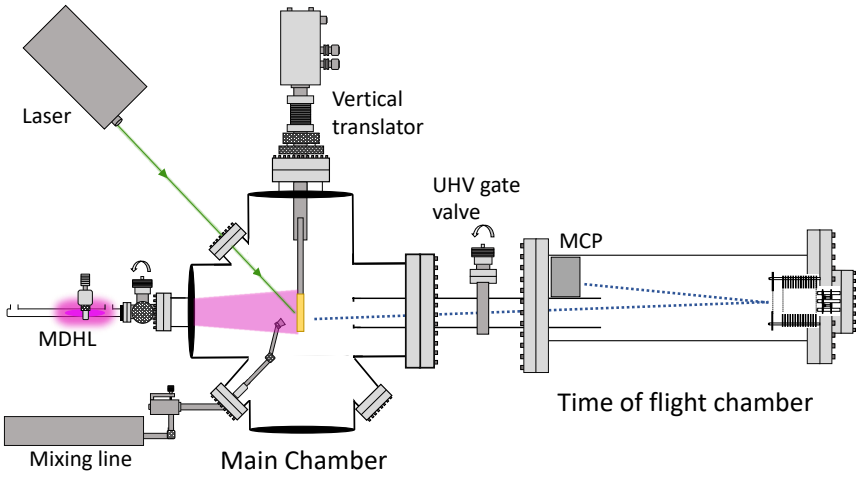

Figure 2.2: *Schematic, not-to-scale, representation of the MATRI^{2}CES setup. The image has been kindly provided by Pranjal Samarth.*

Table 2.1: *Band strengths used in this paper taken from literature.*

Mode	Wavenumber cm^{-1}	Band strength cm $molec^{-1}$	Reference
^{12}CO, CO-stretch	2139	1.4E-17	Bouilloud 2015 [17]
^{13}CO, CO-stretch	2092	1.32E-17	Bouilloud 2015 [17]
H_2S, HS stretch	2547	$(1.69 \pm 0.08) \times 10^{-17}$	Yarnall 2022 [18]
H_2S_2, HS stretch	2490	$(2.0 \pm 0.4) \times 10^{-17*}$	Cazaux 2022[12]

in absorption features in the measured spectrum. The abundance is obtained using the modified Beer-Lambert law:

$$N = \frac{2.3}{4.5} \frac{\int \tau_\nu d\nu}{A'}. \tag{2.1}$$

Here N is the column density of the ice. $\int \tau_\nu d\nu$ is the integrated absorbance of the peak and A' is the apparent band strength of the molecule. The band strengths used in this research are shown in Table 2.1. Band strengths are measured in transmission mode, meaning that the light passes through the ice just once. CRYOPAD2 uses RAIRS in which light passes through the ice, gets reflected at the gold substrate surface and then passes through the ice again. This increases the sensitivity since the path through the ice is longer, but it means that the band strengths need to be corrected. A correction factor of 4.5 was measured previously by N.F.W. Ligterink[15]. The factor of 2.3 is necessary to convert from absorbance to optical depth. Furthermore, as Teolis 2007[16] showed, the band strength is not constant for different ice thicknesses in the RAIRS configuration. For thin ices the relation between column density and ice thickness is linear, but it ceases to be linear for thicker ices. Therefore it is important to confirm that the ice is indeed in its linear regime.

2.1.2 Quadrupole mass spectrometer

The quadrupole mass spectrometer (QMS) is used to analyze the ionic species and their fragments in the gas phase. After ionization by the electrons (70eV), the ions are guided through the mass filter towards a SEM (Secondary Electron Multiplier) which significantly increases the signal before it is measured at the detector. The mass filter only lets the desired mass-to-charge ratio (m/z) through at a time. Since all ions have a charge of $+1^\dagger$, the mass of the fragment can be determined directly. The mass filter can be quickly adjusted to let

†Double ionization is possible, but it only accounts for a fraction of total signals.

Version of June 22, 2023– Created June 22, 2023 - 08:12

through a different mass which gives the ability to monitor the multiple masses during experiments. The detector only measures a raw count which can be used to compare the ratios between different m/z, but it does not directly yield the number density of the molecules in the gas phase. To quantify the number density of the molecules present the signal is corrected in the following way:

$$N = k_{QMS} \frac{A}{IF * FF * S * \sigma^{+}}. \tag{2.2}$$

Here N is the column density that represents the amount of species desorbed per surface area. k_{QMS} is a correction factor for the QMS (see below). A is the QMS signal integrated over time. IF is the ionization fraction of the molecule and assumed to be 1 for all molecules at 70eV. As mentioned, molecules tend to fragment during the ionization. If the parent molecule (unfragmented molecule) is known and a fragmentation pattern is available, the fragmentation can be accounted for with the fragmentation fraction (FF) of a certain mass with respect to total fragments. S is the sensitivity of the QMS at different m/z and it is unique for each QMS. J. Terwisscha van Scheltinga[14] has measured this Mass Sensitivity Function (MSF) of the applied QMS and provided an empirical equation:

$$S(\mathrm{m/z}) = 1.160 \cdot \exp\{-0.064 \cdot (\mathrm{m/z})\} + 0.009 \tag{2.3}$$

Finally, the σ^{+} is the ionization cross-section of the molecule and can be borrowed from literature.
To get the k_{QMS} calibration factor, we need to perform an experiment where we know exactly how many molecules have desorbed. For this we use the CO photodesorption rate. CO does not undergo any photodissociation as the applied UV photon energy is lower than the threshold energy (11.2 eV), and has negligible CO2 formation through excited CO. Therefore, the decrease in CO signal in column density measured by IR is directly proportional to the QMS signal. This experiment will be described in more detail in Section 2.1.7.

2.1.3 Experiments overview

Three experiments were performed on CRYOPAD2, see table 2.2. . Experiment 1 is the main experiment meant to measure the effects of UV irradiation on H_2S ice and experiment 2 was used to study the desorption temperature of H_2S ice for reference. Both experiments concluded with a TPD to 300K. Experiment 3 is used to calibrate the QMS signal based on the CO photodesorption rate determined by the IR spectrum. This gives the conversion factor between QMS count and actual amount of substance.

Table 2.2: *Experiments performed on CRYOPAD2*

Experiment	Description	Irradiation time	TPD
Experiment 1	H_2S + UV	60 minutes	5 K/min
Experiment 2	H_2S	none	5 K/min
Experiment 3	CO	60 minutes	none

2.1.4 Deposition

The ices are formed by letting pure H_2S gas into the main chamber which then freezes onto the cold substrate (15 K). This process is referred to as deposition. Before deposition, the H_2S gas is stored at 10 mbar in the deposition line and a leak valve controls the flow of gas from the deposition line into the chamber. An indicator on the valve shows much the valve has been opened. This value was kept constant between different experiments. The pressure in the chamber reaches an equilibrium between the inflow and outflow of gas and stays constant during deposition.
The IR spectrum of the ice is measured during deposition using FTIR in order to monitor the deposition rate and abundance in each experiment. Due to the constant gas pressure in the chamber the growth of ice should be linear. This can be used to confirm that the ice is still in its thin regime and that the band strength scales linearly with the column density.

2.1.5 Irradiation

The ice is irradiated using an MDHL that produces UV radiation. The photon flux of this lamp has been measured previously to be 3×10^{13} photons cm^{-2} s^{-1} (Tara Bründl, private communication). The lamp is turned on before the experiment to stabilize the flux and is kept on during the experiment. The shutter gate is only opened for irradiation periods but is closed otherwise to shield the ice from radiation. During irradiation ,multiple processes can take place in the ice (photo(chemical) desorption, photodissociation and formation of new products due to recombination). These ongoing processes are monitored with FTIR and the QMS. The FTIR takes a full spectrum every 5 minutes and enables us to derive the kinetics of formation of new products and the decrease of the parent species. The QMS constantly measures the contents of the gas phase and is used to measure the desorption rate.

2.1.6 Temperature Programmed Desorption

In order to further investigate the photoproducts of the ice, Temperature Programmed Desorption (TPD) experiments are performed. After irradiation, the substrate is warmed at a constant rate of 5 K/min. This heats up the ice so that molecules thermally desorb according to their desorption temperature. The temperature at which the desorption happens differs between molecules and can therefore be used to differentiate between products. During TPD, FTIR measures a full spectrum every 2 minutes which yields an IR spectrum every 10K. The QMS monitors relevant masses during the warming process and determines the desorption temperatures of products as the temporal resolution is much higher than the FTIR.

2.1.7 QMS calibration

As mentioned in Section 2.1.2, the calibration factor k_{QMS} must be determined in order to quantify the QMS signal in terms of desorbed molecules from surface area. For this we determined the photodesorption rate of CO ice using FTIR spectroscopy. CO does not undergo any photodissociation when hit by UV radiation, so the decrease of the IR absorption can be fully correlated to the detected QMS signal. The k_{QMS} factor in equation 2.2 is obtained by taking the ratio of column density (N) over integrated QMS signal.

2.2 MATRI^{2}CES

This section will further describe the analytical method of MATRI^{2}CES and the experiments performed on this setup. MATRI^{2}CES uses time-of-flight mass spectrometry (TOF-MS) combined with laser ablation and post ionization in order to study the ice chemistry taking place on the substrate. This technique has multiple steps which will be described in order along with the relevant details of the setup itself. These steps are: laser ablation, ionization, ion extraction, TOF and ion detection. For simplicity this will be referred to as ion creation (ablation, ionization, extraction) and ion detection (TOF, ion detection). The setup contains two vacuum chambers that are divided by a UHV gate valve. The main chamber is used to study ice and ion creation of the ices and the second chamber is used for TOF. For further technical description please refer to the latest version of MichaÅ Bulak's PhD thesis[19].

2.2.1 Ion creation

MATRI^{2}CES has a unique way of analyzing the ice as the laser beam (ca.1 mm) only samples/scans through column of the substrate for each measurement. The current gold substrate has a width of 7 mm leading to four columns that can be used for experiments along with two testing spots on the edges of the gold. In order to measure a fresh ice spot each time, substrate is installed on linear manipulator and moved in sync with the laser. For each mass spectrum measurement of the ice, 70 spots on a single column are scanned and then averaged in order to increase the signal-to-noise ratio. The laser's repeated rate is 5 Hz and the ion creation and ion detection steps are executed each time.
When the ice is hit by the laser, it instantly desorbs and forms a gas plume that quickly sublimate from the substrate. An electron beam that intersects with the substrate ionizes the gas plume and forms cations. Two electronically charged plates positioned on either side of the plume. When a potential difference is applied between these two plates, the ions are pushed towards the TOF tube. Here multiple electronic plates are used to focus and guide the ion beam into the TOF chamber at a slight angle.
The exact timings and the voltages of the electronic plates are crucial in order to receive a good mass spectrum. The voltages of the ion optics have been calibrated, however timing of the extraction plate is adjusted to optimize for signals of molecules studied in this work. The velocity of the gas plume is dependent by the masses of the molecules and it is not homogeneous. Since the extraction plate is only turned on for a short pulse, the plume is only partially extracted. For this project, the timing was optimized for H_2S detection. The process is further described in Section 2.2.4.

2.2.2 Ion detection

As the ions are sent into the TOF tube, the ions become are separated according to their mass as larger molecules accelerate slower than small molecules. The TOF is operated in reflectron mode meaning the ions are reflected at the end of the tube by another electronic plate and accelerated back at a slight angle towards the detector. The detector is a Multichannel Plate sensor (MCP) that amplifies the signal much like a SEM. The voltage across the MCP can be varied to increase or decrease the sensitivity. It is important to not saturate the MCP as this could permanently damage it. Therefore the MCP voltage is varied based on the thickness of the ice in order to find the balance between a good signal-to-noise ratio and a working MCP.

2.2.3 Experiment overview

Due to the high detection sensitivity and theoretical unlimited mass range of TOF, photolysis experiments were performed on MATRI^{2}CES. Various ideas were explored for this project, some of which will be described here. As this is the first time that H_2S is used on this setup, some calibration experiments were needed to ensure that the signal-to-noise ratio is increased as much as possible. For this the deposition parameters needed to be found (Section 2.2.5) as well as the extraction plate timing (Section 2.2.4). We investigated kinetics of UV irradiation of H_2S (Section 2.3) and quantified the photo-products (Section 2.2.7). Finally we also varied the ionization voltage of the electron gun in order to aid in separating hydrogenated sulfur chains from pure sulfur rings (Section 2.2.8).

2.2.4 Plume Profiles

The optimal extraction plate timing was determined by creating so-called plume profiles. These profiles show the change in signal intensity as a function of time. Instead of using 70 spots to create a single mass spectrum, part of the column is used to determine the average mass spectrum for one extraction setting. To be precise, 100 spots are ablated in total and 10 timings are checked meaning that each spectrum is an average of 10 spots. The best timing is then used for subsequent experiments. As H_2S is the main species of interest, the timing was chosen to maximize the H_2S signal.

2.2.5 Deposition

The general deposition procedure is the same as on CRYOPAD2 (see Section 2.1.4). The deposition line pressure, leak valve value and deposition duration are kept constant in each experiment. Water, which has a similar structure to H_2S was used as a guideline to find suitable deposition settings. The deposition line pressure was chosen to the same as for water (20 mbar). Then the leak valve position was selected in order to achieve the same deposition pressure in the main chamber as water (2.0×10^{-8} mbar). And finally, the duration of deposition was chosen to achieve a good signal at an MCP voltage of 2525‡.
There is no way to precisely determine the thickness of the ice on MATRI^{2}CES as the conversion factor from MCP signal to number density is unknown. Furthermore, the exact measurement parameters have a large effect on the received

‡This is a voltage used often on MATRI^{2}CES and it was selected as the preferred voltage for most experiments.

signal and it is difficult to characterize these effect. Still, we can find an upper limit on the ice thickness using the Langmuir approximation. If we assume that every molecule that hits the surface gets adsorbed, then the thickness of the ice can be determined from the pressure in the chamber in the following way:

$$N[\text{ML}] = P[10^{-6}\text{Torr}] \cdot t[\text{s}] \tag{2.4}$$

Here N is the ice thickness in ML, P the chamber pressure in units of Torr (1 Torr = 1.33 mbar)[§] and t the deposition time in seconds. Since not all molecules will stick to the surface, this provides an upper limit on the ice thickness. The pressure P is measured at room temperature where no adsorption takes place.

2.2.6 Irradiation kinetics

The change in quantity of species during irradiation (either through formation or destruction) will be referred to as 'kinetics'. As MATRI^{2}CES is able to perform multiple measurement on a single ice, accurate measurements of kinetics can be performed by measuring a single column in-between irradiation intervals. In order to be able to better compare multiple days of experiments, a reference spectrum is also taken for no irradiation and all measurements were performed at a MCP voltage of 2525. An overview of irradiation times can be seen in table 2.3. The flux of the MDHL was measured to be $(2.5 \pm 0.5) \times 10^{14}$ photons cm^{-2} s^{-1}[19].

Table 2.3: *Overview of irradiation experiments performed on MATRI^{2}CES. KIN-short, KIN-medium and KIN-long measured at an MCP voltage of 2525 V. KIN-20 was measured at 2750 V.*

Experiment	Description	Ionization voltage (eV)	Irradiation durations
Experiment 4_KIN-short	H_2S + UV	70	0 s, 10 s, 20 s, 40 s
Experiment 5_KIN-medium	H_2S + UV	70	0 s, 40 s, 80 s, 160 s
Experiment 6_KIN-long	H_2S + UV	70	0 s, 8 min, 32 min, 64 min
Experiment 7_KIN-20	H_2S + UV	20	1 min, 2 min, 8 min

2.2.7 Step warming

The proper identification of products using laser ablated mass spectrometry is difficult because all species (parent and products) desorb and fragment at the

[§]1 Torr is defined to be exactly $\frac{1}{760}$ atm

same time. The large photoproducts of H_2S (H_2S_x and S_x, $1 \leq x \leq 6$) create fragments which share the same structure as smaller photoproducts. Furthermore, only the fragmentation patterns of H_2S, S_6 and S_8 are available from the NIST webbook. Furthermore the H_2S_2 mass spectrum has been provided by Julia de Carvalho Santos through private communication.
After UV irradiation of H_2S ice sample for 64 min, we performed step warming rather than TPD which enabled us to measure spectra at specific temperatures. This enables us to isolate different S-bearing products. An overview can be found in table 2.4. In order to desorb as much of the product as possible the setup was kept at the desired temperature, i.e. few K above the desorption temperature of the species of interest, until the pressure in the chamber returned to a constant value below 10^{-8} mbar. As the ice sample was irradiated, a large part of the H_2S was either photoprocessed or photochemically desorbed. This meant that the MCP voltage could be increased without saturating the MCP. This leads to a better signal-to-noise ratio for larger products.

Table 2.4: *Overview of temperatures at which an irradiated H_2S ice sample was measured. The sample had been irradiated for 64 minutes prior to measurement using an MCP voltage of 2775.*

Experiment	Description	Irradiation time	Temperatures (K)
Experiment 8_SW-low	H_2S + UV	64 min	15, 100, 143, 175
Experiment 9_SW-high	H_2S + UV	64 min	15, 170, 220, 275

2.2.8 Ionization voltage

To further help distinguish between product and fragment, we explored the option of lowering the ionization voltage of the electron gun in order to reduce fragmentation. Usually measurements are taken with ionization of 70 eV which is the energy for the maximum ionization cross section. However, it generates more fragments than lower ionization energy. Lowering the voltage means that less energy is transferred to the molecules and breaking the molecular bonds becomes less efficient. Another consequence is that there is less ionization in general which decreases the signal. Irradiation and step warming experiments were performed at an ionization voltage of 20 eV, which is the lowest voltage at which experiments have been performed on MATRI^{2}CES.

Chapter 3

Results

This chapter will present the results of the performed experiments. Results obtained from CRYOPAD2 experiments are shown in Section 3.1: deposition (3.1.1), QMS calibration (3.1.2), irradiation (3.1.3) and TPD (3.1.4). Section 3.2 presents results obtained on MATRI^{2}CES: plume profiles (3.2.1), deposition (3.2.2), irradiation (3.2.3) and step warming (3.2.4).

3.1 CRYOPAD2

3.1.1 Deposition

As mentioned previously, we must confirm the ice is in a 'thin-ice' regime so the corrected RAIRS band strengths can be used to derive the absolute abundance. By measuring the ice during deposition we can monitor this behaviour. Figure 3.1 (a) shows column densities of ^{12}CO and ^{13}CO obtained by integrating the stretching mode peaks and applying the modified Beer-Lambert law formula (eq. 2.1). The integration windows were kept constant for each of the peaks. Carbon (C) appears in nature largely as ^{12}C, meaning the carbon atom has a total mass of 12 u. A small fraction is found as ^{13}C (1.07% of total carbon[20]). The ^{12}CO peak tapers off after 5 minutes of deposition and ceases to represent a linear correlation between absorbance area and abundance. The ^{13}CO peak does not show such drastic behaviour. Therefore, total CO column density is derived by correcting the ^{13}CO column density by its natural abundance:

$$N(CO_{tot}) = \frac{N(^{13}CO)}{0.0107} \tag{3.1}$$

During deposition the leak valve was kept at the same position yielding a constant deposition pressure of 3.2×10^{-8} mbar in the main chamber. The deposi-

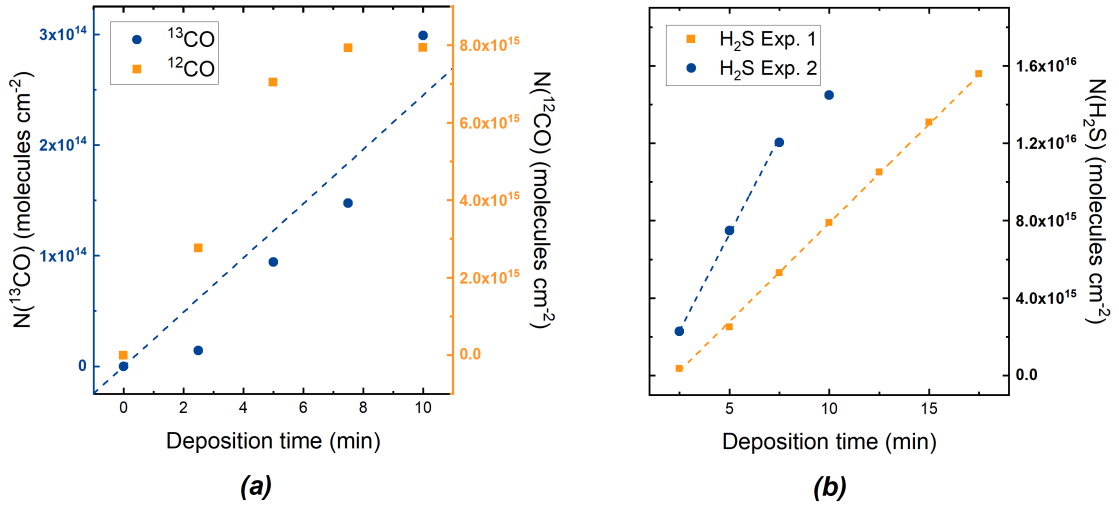

Figure 3.1: *(a) Column densities of ^{13}CO and ^{12}CO during the deposition of CO ice. The straight line is a linear fit through (0,0) meant as a visual guide. (b) Column density of H_2S during the depositions of Exp. 1 and Exp. 2 (Table 2.2). The dashed lines are linear fits meant as visual guides.*

tions of H_2S for Exp. 1 and Exp. 2 are shown in the right panel of Figure 3.1. experiment 2 shows linear deposition until the desired thickness is reached (15 ML) meaning that the band strengths still apply. During Exp. 2 the deposition rate was higher, but reached the same total H_2S abundance. The difference in deposition rate is probably due to a slight change in the leak valve precision after usage. This was adjusted for during deposition.

3.1.2 QMS calibration using CO

The following section presents the results and analysis of the CO photodesorption experiment used to determine the k_{QMS} factor which is subsequently used to quantify the H_2S signal in the QMS.
Irradiation was performed in intervals of 10, 10, 20, 20 and 135 minutes with breaks of either 10 or 20 minutes in-between. Since the ^{12}CO IR peak is not correlate with the absolute abundance of total carbon monoxide, we only use 13CO for deriving the photodesorption rate through natural isotope ratio correction. Figure 3.2 (a) shows a nearly linear depletion of ^{13}CO as a function of time. The shadowed areas correspond to irradiation intervals during which the shutter was open. Most photodesorption values in literature only report the ^{12}CO photodesorption rate, but to properly link the IR to the QMS we need to consider the total CO photodesorption (^{12}CO + ^{13}CO) as the fragmentation fraction (FF, taken from NIST webbook) accounts for all CO fragments

(not just 12C and ^{16}O). The data points taken during irradiation (shaded area in Figure 3.2) are extracted into Figure 3.2 and a linear fit is applied yielding the following photodesorption rates: $(3.43 \pm 0.07) \times 10^{-2}$ for ^{12}CO + ^{13}CO and $(3.40 \pm 0.06) \times 10^{-2}$ for ^{12}CO per incident photon. We define IR_{slope} to be the desorption rate of total CO. The measured ^{12}CO photodesorption rate is in good agreement with the photodesorption rate measured by Muñoz Caro et al. (2016)[21] at 15 K.
During the UV irradiation of CO ice, ^{12}CO desorption (28 m/z) is constantly probed by the QMS. There is a significant increase QMS signal when UV photons irradiate the ice, but it is not a neat block function, see Figure 3.3 (a). Instead a slow increase can be seen during irradiation, and then a decreasing tail after the shutter is closed. This tail was not included in within the integration limits as it did not lead to a significant increase in the desorbed signal. The separate irradiation intervals are integrated and corrected using the QMS correction formula (see eq. 2.2) with $FF = 0.92$ and σ^+ =2.44 Å^2[22]. Figure 3.3, right panel, shows the total cumulated signal along with a linear fit with a slope (QMS_{slope}) of $(4.6 \pm 0.2) \times 10^{-11}$ corrected count photon^{-1} cm^{-2}. k_{QMS} is then determined with

$$k_{QMS} = \frac{IR_{slope}}{QMS_{slope}} \tag{3.2}$$

with IR_{slope} the total photodesorption rate of CO and QMS_{slope} the QMS linear fit. This yields a calibration factor k_{QMS} of $(7.5 \pm 0.4) \times 10^8$ for the applied QMS on CRYOPAD2.

3.1.3 UV irradiation

As the H_2S ice is irradiated, the ice abundance of H_2S will decrease due to desorption and photoconversion forming other S-bearing products. Figure 3.4 shows the decrease in the 2556 cm^{-1} peak which corresponds to HS stretching modes of amorphous H_2S ice. After 60 minutes irradiation the peak has not stabilized, but the rate of decrease has slowed. At the same time a new peak is formed at 2494 cm^{-1} corresponding to the HS stretching mode of H_2S_2[12]. This peak reaches it's maximum value within the first 5 minutes of irradiation leading to a constant peak in the difference spectrum (Figure 3.4(b)). The final H_2S_2/H_2S ratio achieved is 0.5 ± 0.1.
The photochemical desorption and photodissociation rates of H_2S were further explored by analyzing the decrease of the IR peak. The peak area is calculated by integrating under the curve without any Gaussian fitting and converted to column density using using eq. 2.1 as shown in Figure 3.6. As UV photons are

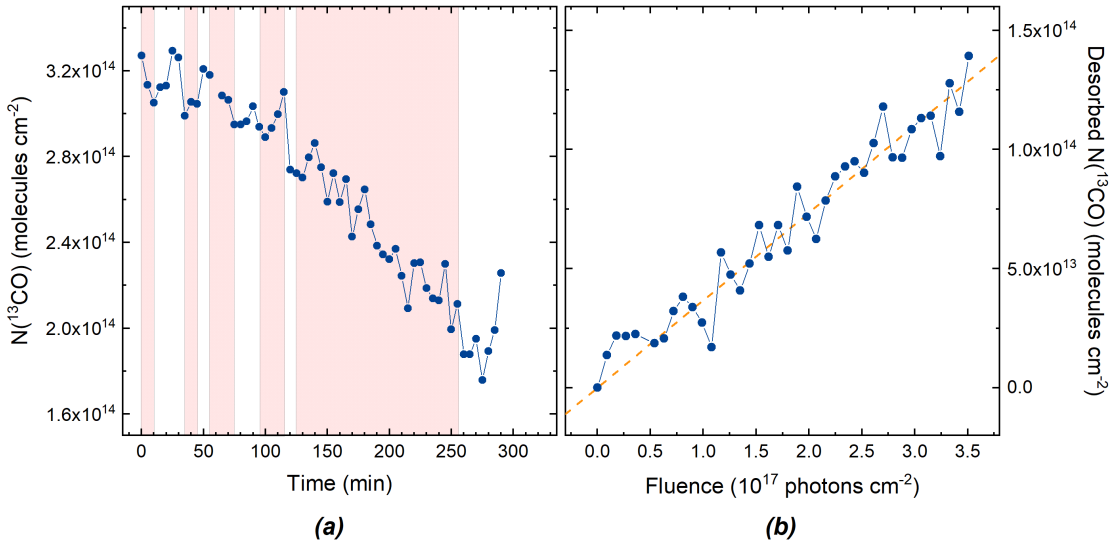

Figure 3.2: *(a) ^{13}CO column density during irradiation. Shaded areas correspond to irradiation intervals. (b) The irradiation data points (within the shaded areas) are extracted and re-scaled to show the total desorbed ^{13}CO column density. The solid line represents a linear fit through (0,0) with a* $= (3.67 \pm 0.08) \times 10^{-4}$ *molecules photon*$^{-1}$.

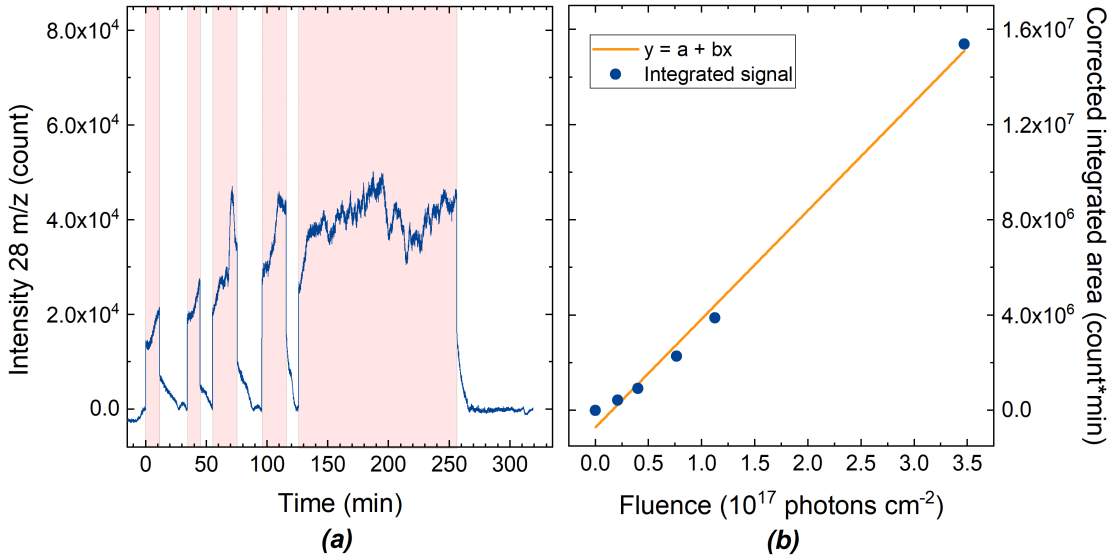

Figure 3.3: *(a): Signal intensity of 28 m/z measured by the QMS during irradiation of CO ice. Baseline has been subtracted. Shaded areas represent irradiation intervals. (b) Cumulated sum of the integrated shaded areas in the left panel corrected as described in the text. The linear fit is: a=* $(4.6 \pm 0.2) \times 10^{-11}$*, b=* $(-7 \pm 3) \times 10^{5}$

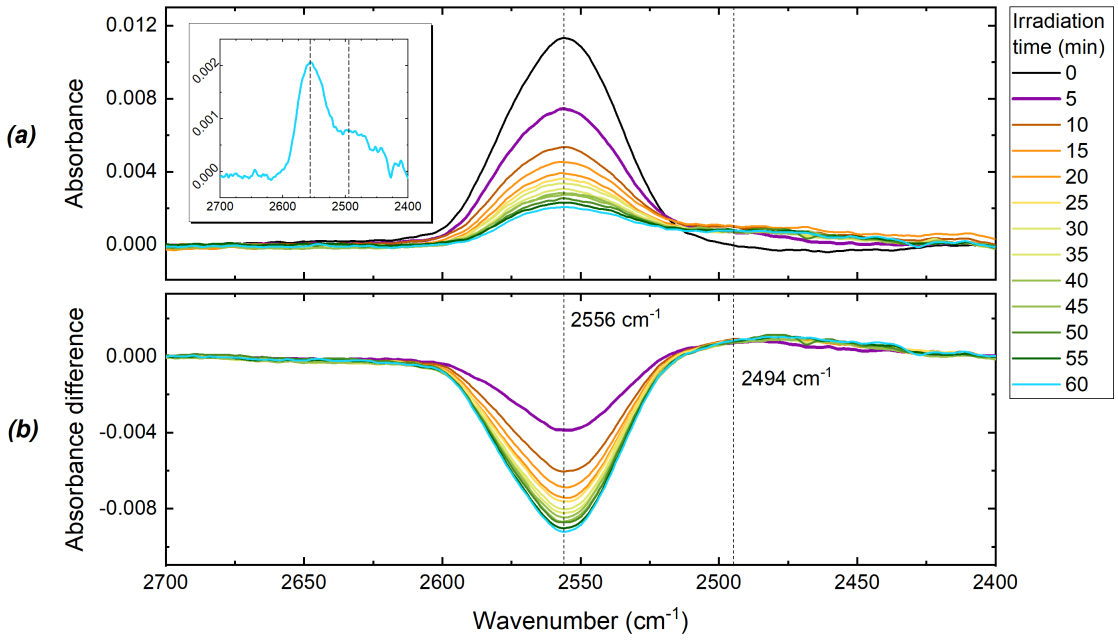

Figure 3.4: *(a) IR spectra of H_2S ice during irradiation. The inset on the top-left shows the IR spectrum after 60 min of irradiation. The dashed lines correspond to the HS-stretching modes of H_2S (2556 cm^{-1}) and H_2S_2 (2494 cm^{-1}). (b) Absorbance differences between the irradiated ices (starting from 5 min irradiation) and the reference ice at 0 min irradiation.*

able enter the ice, photodissociation can be expressed as a pseudo first-order which depends on the initial ice column density, while the photochemical desorption is a zero-order reaction. Solving this differential equation results in an exponential decrease of H_2S. The fit in Figure 3.6 is therefore a combination of a linear (photochemical desorption) and an exponential (photodissociation) process. This yields a linear desorption rate of 0.034 ± 0.002 molecules per incident photon and a photodissociation cross section of $(9.3 \pm 0.5) \times 10^{-17}$. However, this is not a unique solution for solving these two different mechanisms.
The QMS signal for 34 m/z was used to exclusively derive the desorption of H_2S during irradiation given the gas-phase detection of H_2S directly originates from desorption event. The data calibration is the same as described for CO (Section 3.1.2) using an ionization cross-section of 3.92 $Å^2$[23] and a fragmentation fraction of 0.518 as taken from the NIST database. The 34 m/z signal and the corresponding desorbed column densities are shown in Figure 3.5. A linear fit to the column densities yields a desorption rate of $(3.3 \pm 0.3) \times 10^{-3}$ molecules per incident photon.

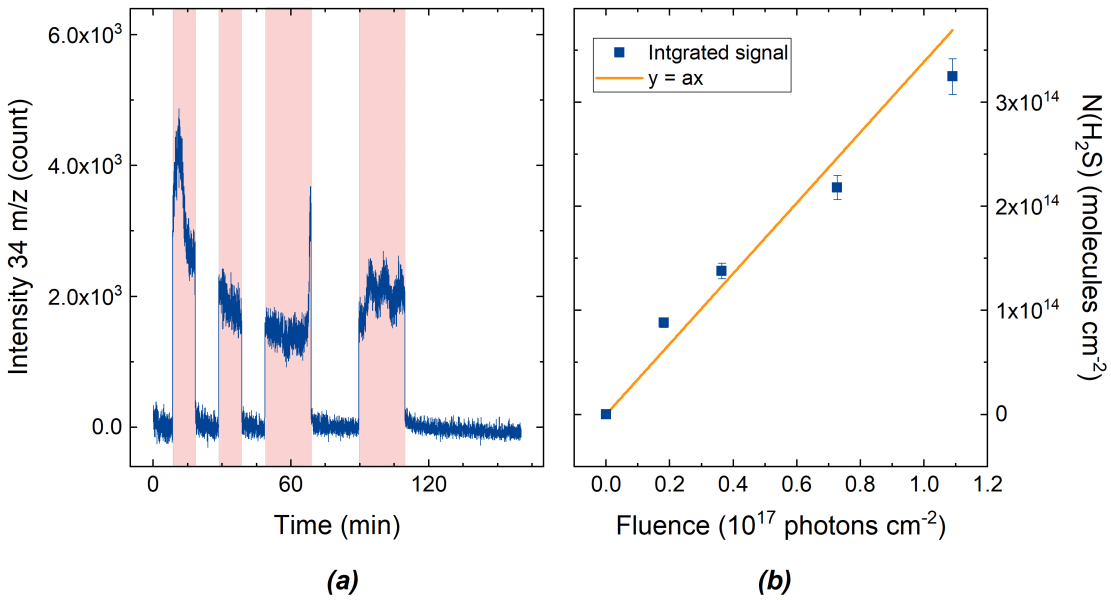

Figure 3.5: *(a) Signal intensity of 34 m/z measured by the QMS during irradiation of H_2S ice. (b) Corresponding column density calculated using eq. 2.2 as described in the text. The k_{QMS} uncertainty is propagated to the column densities. The solid line has a slope of $(3.3 \pm 0.3) \times 10^{-3}$.*

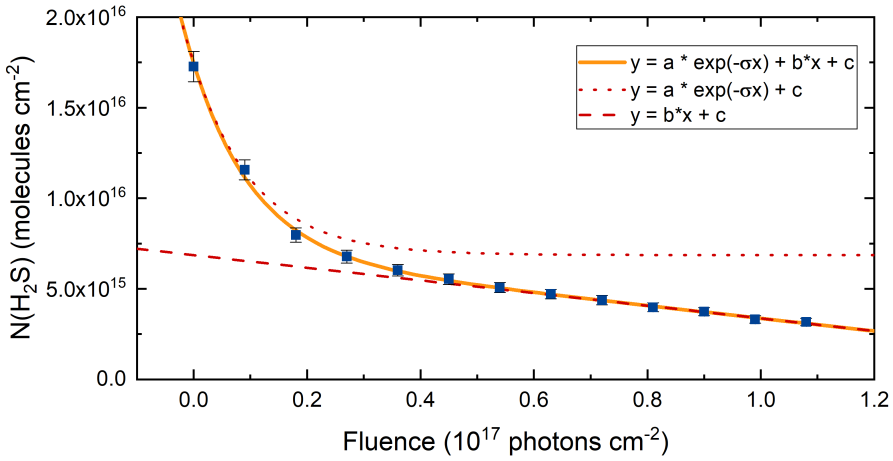

Figure 3.6: *Data points represent the column densities of the H_2S ice during irradiation with the propagated band strength and Gaussian fit uncertainties. The solid line represents a combination fit of an exponential and a linear function (see legend) with the following parameters: $a = (1.06 \pm 0.03) \times 10^{16}$, $b = (-0.034 \pm 0.002)$, $c = (6.9 \pm 0.2) \times 10^{15}$ and $\sigma = (9.3 \pm 0.5) \times 10^{-17}$. The dotted and dashed lines represent the exponential and linear parts of the fit respectively.*

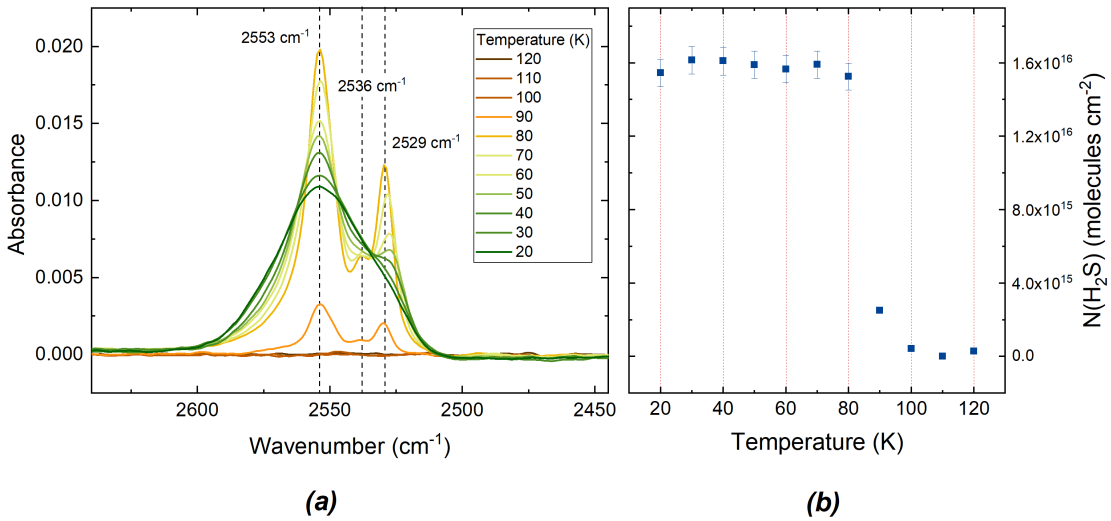

Figure 3.7: *(a) IR spectra of unirradiated H_2S ice during TPD. Peaks are described in the text. (b) Column density of H_2S during TPD calculated by integrating the IR spectrum. Uncertainty in column density is due to band strength uncertainty.*

3.1.4 Temperature Programmed Desorption

A Temperature Programmed Desorption (TPD) experiment was performed on an unirradiated H_2S ice sample. During the heating process crystallization of H_2S was visible in the IR spectrum (Figure 3.7 (a)) at 40 K. Two prominent peaks at 80 K (2553 cm^{-1} and 2529 cm^{-1}) correspond to the asymmetric and symmetric HS stretching modes of H_2S, respectively. The small peak at 2536 cm^{-1} could be due to leftover H_2S ice[7]. All peaks drastically decrease between 80 K and 90 K due to thermal desorption and completely disappear at 100 K. The QMS data confirms this with a desorption peak at 85K for both 34 m/z (H_2S or ^{34}S) and 32 m/z (S) (not shown here). Comparing the integrated area of the desorption peaks we get a 34/32 ratio of 2.5, which matches the NIST mass spectrum data of H_2S.

TPD was also performed on the irradiated sample. Due to photo(chemical) desorption and photodissociation the H_2S peak intensity is significantly less than the unirradiated peak as shown in figure Figure 3.8. The 2556 cm^{-1} (H_2S, HS-stretch) and 2494 cm^{-1} (H_2S_2, HS-stretch) were deconvoluted using a Gaussian fit to the data. No crystallization of the H_2S is observed during warming, probably due to the formation S-bearing products in the ice sample or the small peak intensity. The main decrease in H_2S happens between 80 K and 100 K. The H_2S_2 peak slightly decreases as H_2S is desorbing, but depletes significantly between 140 K and 150 K.
The QMS signal confirms the desorption temperatures of the above species (Fig-

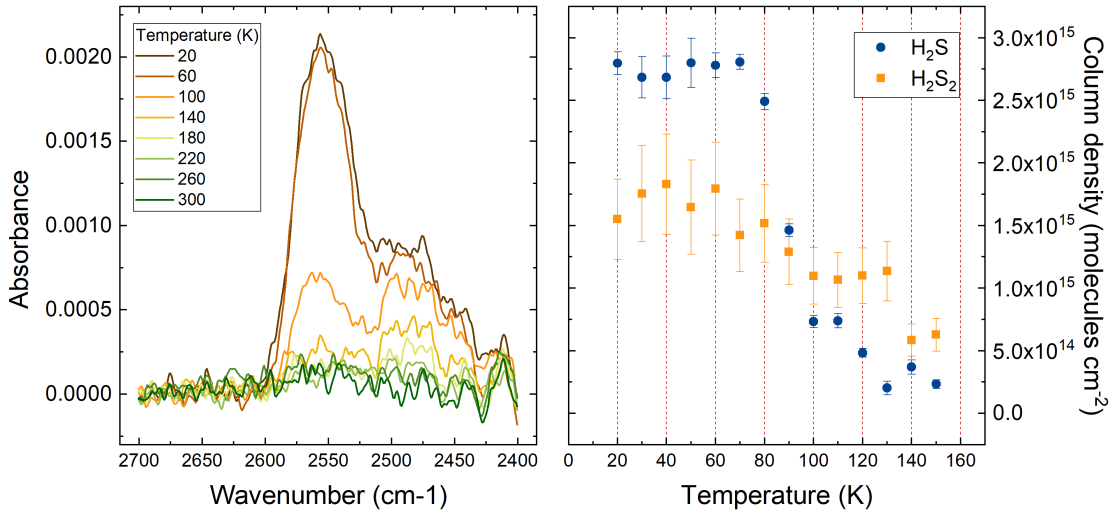

Figure 3.8: `Left panel:` *IR spectra of irradiated H_2S ice during TPD.* `Right panel:` *Column density of H_2S and H_2S_2 during TPD calculated using a double Gaussian fit to the IR spectra. Uncertainties are due to the Gaussian fit and the band strength uncertainties.*

ure 3.9). The main H_2S peak is at 8 5K and the H_2S_2 peak is at 142 K. Several desorption peaks are seen for H_2S_3 (165 K) and H_2S_4 (215 K). Another desorption peak is present at 265 K, but as the highest mass measured was 160 m/z, which corresponds to S_5, we cannot identify this peak properly. This is likely the H_2S_5 desorption peak. No separate desorption peaks are seen for the pure sulfur allotropes (S_x). These peaks all overlap with desorption peaks of hydrogenated sulfur chains and are most likely fragments. There is another large peak around 200K which most likely due to the desorption of H_2S from other surfaces of the cryostat cold finger. The final small peak of 32 m/z and 34 m/z around 260K is likely due to similar reasons. Figure 3.10 shows the desorption temperatures for the observed hydrogenated sulfur chains, further supporting the claim that H_2S_5 desorbs at 265 K.

3.2 MATRI^{2}CES

3.2.1 Plume Profiles

In order to find the optimal extraction plate timing, first a broad range of timings was probed and then a finer range close to the best value. In order to determine signal intensity, the area of the strongest fragmentation peak (m/z=34) was calculated. The results of the two measurements can be seen in Figure 3.11.

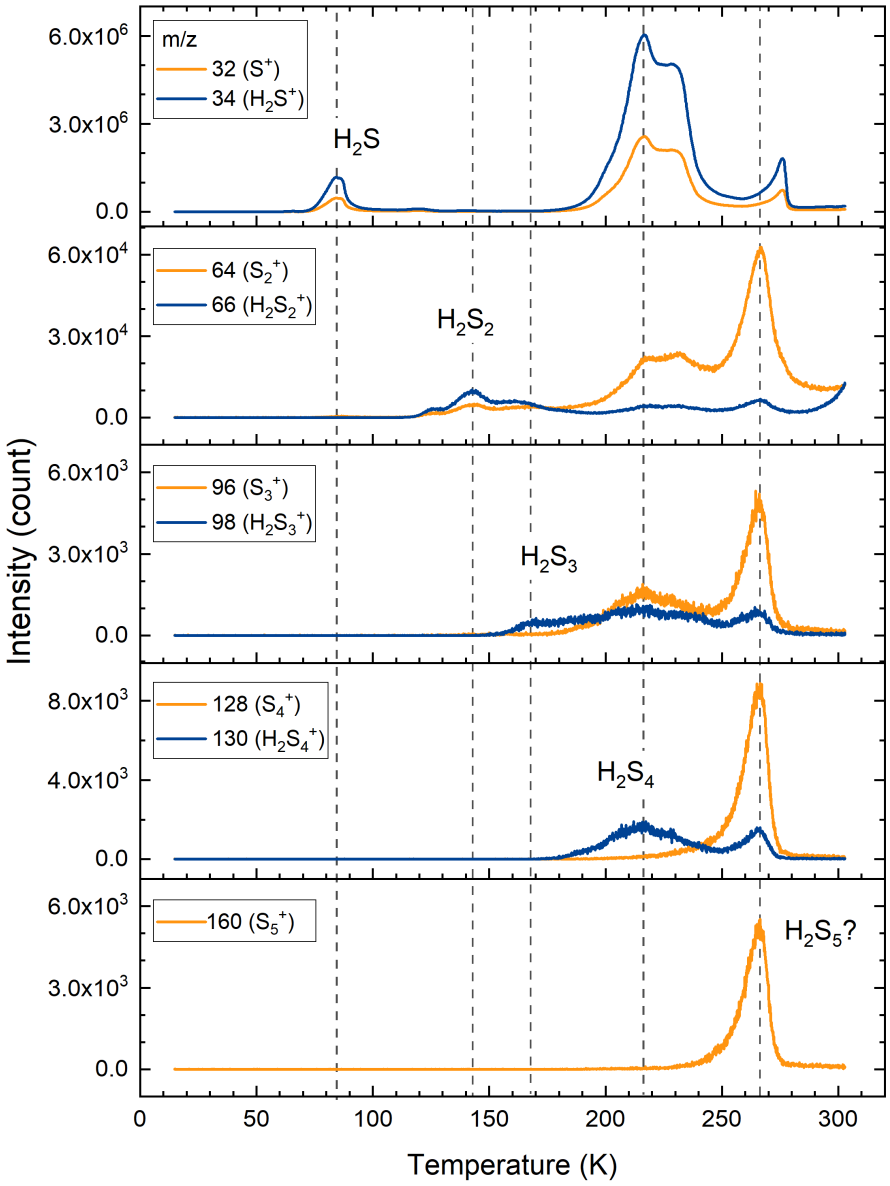

Figure 3.9: *QMS signal intensities for relevant masses during TPD of irradiated H_2S ice. Different mass ranges are split between panels for easier viewing. Desorption temperatures are identified based on the first desorption peak of a certain mass. Later desorption peaks of the same mass are considered to be fragments. The dashed lines show the identified desorption peaks.*

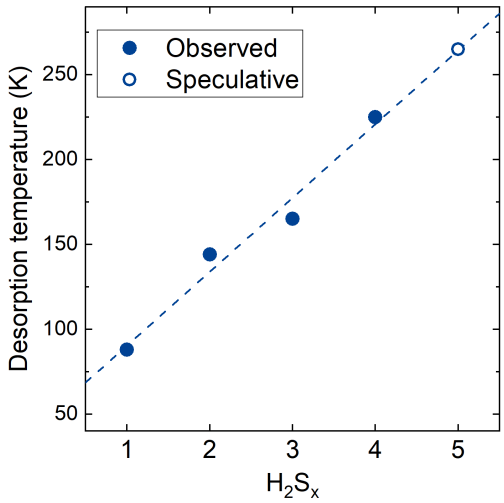

Figure 3.10: *Desorption temperatures of hydrogenated sulfur chains. X-axis depicts the number of sulfur atoms in the molecule. The closed markers have been directly observed and the open marker is only speculated based on the fragments. The dashed line is for visual aid only.*

As the plume profiles were measured for two different ices, the intensities of the peaks do not necessarily overlap. The broad profile shows a peak at 215 µs and the fine profile a peak at 218 µs. The discrepancy is small, but due to the jagged profile of finer profile it was decided to use 215 µs as timing for later experiments. We keep the timing consistent between future experiments, in order to have reproducibility. Both profiles were measured on the same spot at the edge of the substrate which could explain the unevenness of the profile.

3.2.2 Deposition

A leak valve (with an index value of 15.45) was used to yield a deposition pressure that fluctuated between 1.8×10^{-8} and 2.0×10^{-8} mbar in the main chamber. Figure 3.12 shows that this results in a linear deposition of H_2S ice. This is further supported by a Pearson's r value that is close to 1 (0.996) indicating a strong linear correlation. It was decided to use a deposition duration of 20 minutes for further experiments as this resulted in a strong signal which averaged at 60% of the maximum allowed signal value of the MCP. The deposition pressure in the chamber was 1.3×10^{-7} mbar (0.1×10^{-6} Torr) at room temperature. A deposition of 20 minutes yields an upper limit of 120 ML on the ice thickness according to Langmuir estimation (eq. 2.4). In order to compare multiple columns of the same ice sample, the ice thickness must be uniform across the whole width of the substrate. Three tests were performed in order to determine

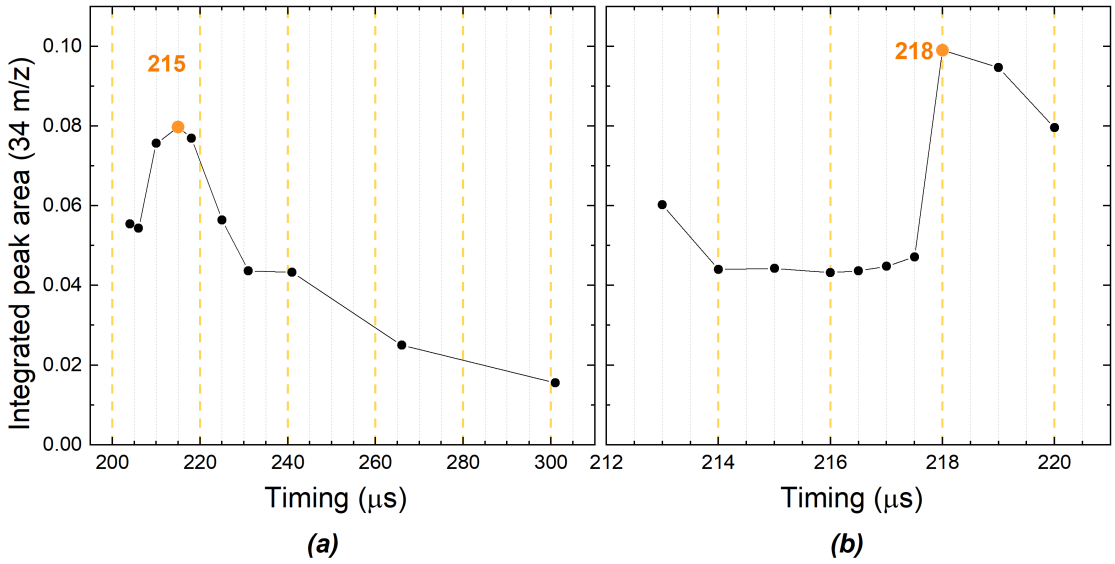

Figure 3.11: *Plume profiles of unirradiated H_2S ice. The intensity of the 34 m/z peak (H_2S molecular ion) is plotted as a function of the extraction time of the ion optic plates.* `(a)` *10 timings used between* 204 µs *and* 301 µs. `(b)` *10 timings used between* 213 µs *and* 220 µs.

the uncertainty in uniformity: (1) unirradiated ice using an ionization voltage of 70 eV, (2) irradiated ice using a voltage of 70 eV and (3) unirradiated ice using a voltage of 20 eV. Figure 3.13 shows the mass spectra between 32 m/z and 36 m/z for these three ices. The uniformity uncertainties are (1) 1%, (2) 16% and (3) 3%.

3.2.3 UV irradiation

Two processes occur simultaneously during UV irradiation: species destruction and the formation of new products. Measurements were performed at a MCP voltage of 2525 V to avoid the saturation of H_2S signal. A spike in pressure (3 orders of magnitude) was observed every time the shutter was opened after which the pressure quickly decreased to a value of an order of magnitude higher than the usual base pressure of the chamber. After 64 minutes of irradiation only the H_2S and the H_2S_2 peaks were visible as the current MCP's sensitivity setting (applied voltage) was too low to detect higher mass products. Experiments with higher MCP voltage confirm formation of higher mass products (see Figure 3.20) which is discussed later. As mentioned, three separate irradiation experiments were performed. Even though the deposition parameters were kept the same for all, the signal intensities varied. This was corrected

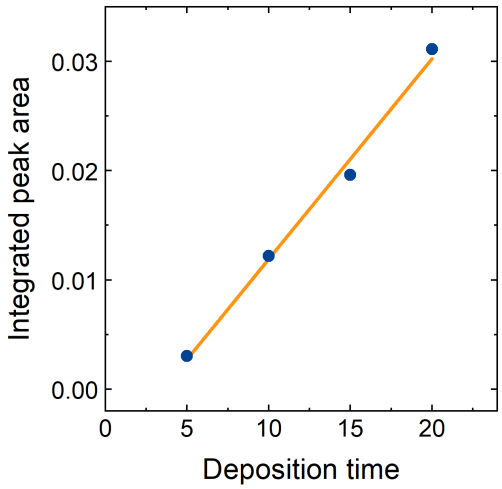

Figure 3.12: *The integrated area of the largest H_2S peak (m/z=34) is shown as a function of the deposition time. Deposition settings are described in the text. The solid line is a linear fit with a Pearson's r value of 0.996*

for using the reference measurements taken before irradiation on all three ices (0 sec, Table 2.3) and scaling all data to the same peak intensity. Figure 3.14 shows segments of the mass spectrum during irradiation. Here all peaks were scaled so that the 34 m/z peak has a maximum value of 1. The decrease in H_2S is seen in in all peaks between 32 m/z and 36 m/z. Furthermore, a cluster of H_2S was observed at 68 m/z that decreases as the parent species H_2S. Figure 3.15 shows the decrease of the 34 m/z peak as the total UV fluence increases. Here the same fit applied as on CRYOPAD2 (Figure 3.6) which yields a photodissociation cross section σ^{ph} of $(9.0 \pm 3.9) \times 10^{-17}$, which is similar to the value derived from the experiment performed in CRYOPAD2.

H_2S_2 and its corresponding fragments (HS_2 and S_2) initially increase during irradiation, but start declining after 10 minutes of irradiation which is shown in Figure 3.16 (b). The peaks were normalized by scaling the intensity of the 34 m/z peak. This results in similar, but not identical, initial peak intensities at 0 min irradiation for each of the masses. The scatter of these peak intensities was used to calculate an uncertainty for each of the masses: 8% (64 m/z), 15% (65 m/z) and 77% (66 m/z). Comparing the KIN-short and KIN-medium experiments (Figure 3.16 (b)) reveals there is no smooth transition from one to the other. The number of irradiation intervals is the main indicator of peak intensity. The spike in chamber pressure as the shutter is opened suggests the initial shock of UV irradiation plays a big role in experimental photochemistry.
In order to quantify the photoproducts of H_2S, a mass spectrum was measured at a higher MCP voltage (Table 2.4 experiment SW2, 15K). This spectrum with

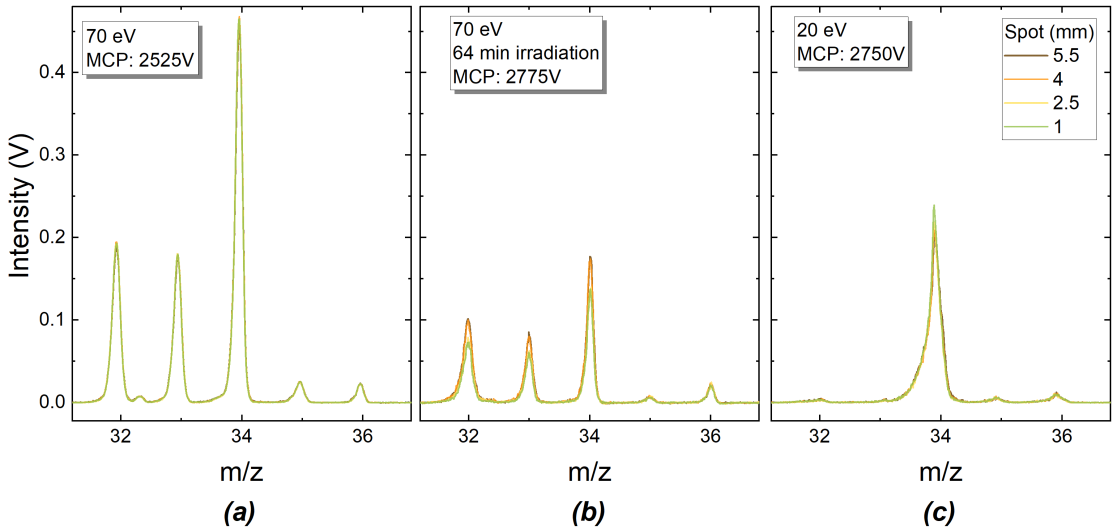

Figure 3.13: *Mass spectra measured at four different columns in order to determine the uniformity uncertainties for three scenarios. Spot in mm depicts the distance between the center of the spot and the substrate edge. (a) Normal parameters. MCP voltage: 2525 V, ionization voltage: 70 eV. (b) Irradiated parameters. MCP voltage: 2775 V, ionization voltage: 70 eV. (c) 20 eV parameters: MCP voltage: 2770 V, ionization voltage: 20 eV.*

higher sensitivity is shown in Figure 3.20 (a). Both hydrogenated and unhydrogenated sulfur chains can be identified, and the highest product is H_2S_6 (194 m/z). However, it remains unclear what is the fragment pattern of each product. The total amount of sulfur atoms present in the ice should be preserved. We aim to report the species composition of total observed products. The amount of unprocessed H_2S was calculated based on an assumption that all 34 m/z signal was only due to H_2S and not fragments of higher-mass products. The contribution of H_2S to its fragmentation masses (m/z = 32, 33, 34, 35, 36) was subtracted from the spectrum resulting in a spectrum that only contains the photoproducts. This spectrum was scaled by the number of sulfur atoms in each species and compared to the leftover amount of H_2S (see Figure 3.17). A total of 1.9 sulfur atoms are stored in photoproducts compared to 1 H_2S molecule in an ice which has received a fluence of $(10 \pm 2) \times 10^{17}$ photons cm^{-2}. A single irradiation experiment was performed at 20 eV which is shown in Figure 3.18. The qualitative results are the same: 34 m/z and 68 m/z peaks decrease in intensity, and the 64 m/z and 66 m/z peaks increase. Due to the difficulty of analyzing 20 eV mass spectra, no further kinetics experiments were performed.
Lowering the ionization does have a significant impact on the fragmentation pattern which can best be seen in Figure 3.13. H_2S (34 m/z) is the most dom-

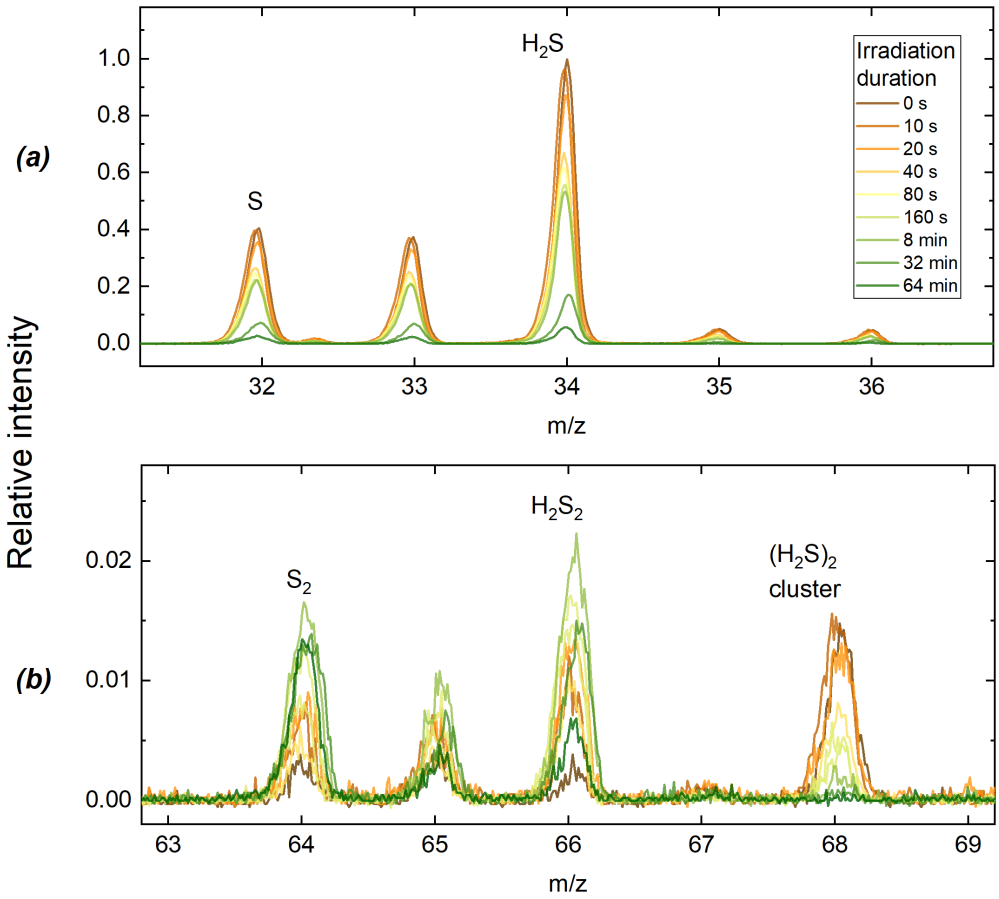

Figure 3.14: *Mass spectrum of H_2S ice during irradiation using 70 eV ionization.* (a) *H_2S fragments.* (b) *H_2S_2 fragments and a H_2S cluster.*

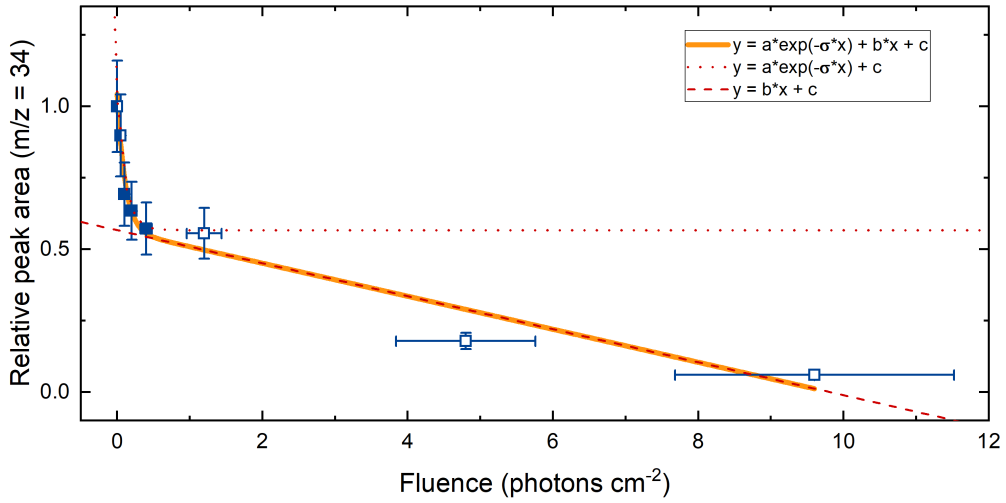

Figure 3.15: *Relative decrease in peak intensity of 34 m/z during irradiation using 70 eV ionization. The x and y uncertainties are due to MDHL flux and uniformity uncertainties respectively. The solid line represent a combination fit of an exponential and a linear function (see legend) with the following parameters:* $a = 0.48 \pm 0.08$, $b = (-5.8 \pm 1.1) \times 10^{-19}$, $c = 0.57 \pm 0.06$ *and* $\sigma = (9.0 \pm 3.9) \times 10^{-17}$. *The dotted and dashed lines represent the exponential and linear parts of the fit respectively.*

inant of the fragmentation and the HS (33 m/z) and S (32 m/z) fragments are barely visible. The largest peak following 34 m/z is 36 m/z which corresponds to the $H_2{}^{34}$Sisotope of H_2S. The 36 m/z fraction of the total H_2S signal (sum of the m/z = 34, 35, 36 peaks) is 4.5%, which close to the natural abundance of ^{34}S: 4.3%[20]. If we compare the H_2S_x / S_x ratios for different masses, we see that this ratio is much lower for the 20 eV spectra (see Figure 3.19 as there is less fragmentation. Crucially, this difference does not aim for quantify the product yield but demonstrates the technique concept of preserving the intact molecular mass.

3.2.4 Step warming

The irradiation experiments provide limited results on the exact species present in the ice due to heavy fragmentation. Therefore the sample was heated in steps in order to sublimate the smaller products (H_2S_x, $1 \leq x \leq 4$) whose desorption temperatures are below 275 K. Figure 3.20 shows the mass spectra of a single irradiated ice at 15 K and warmed up to 275 K. The H_2S (34 m/z) signal, which was the strongest at 15 K, almost entirely disappears at 275 K supports the idea that H_2S desorbs at temperatures below 275 K. Furthermore, after heating the sample S_2 becomes the highest fragment and all unhydrogenated peaks

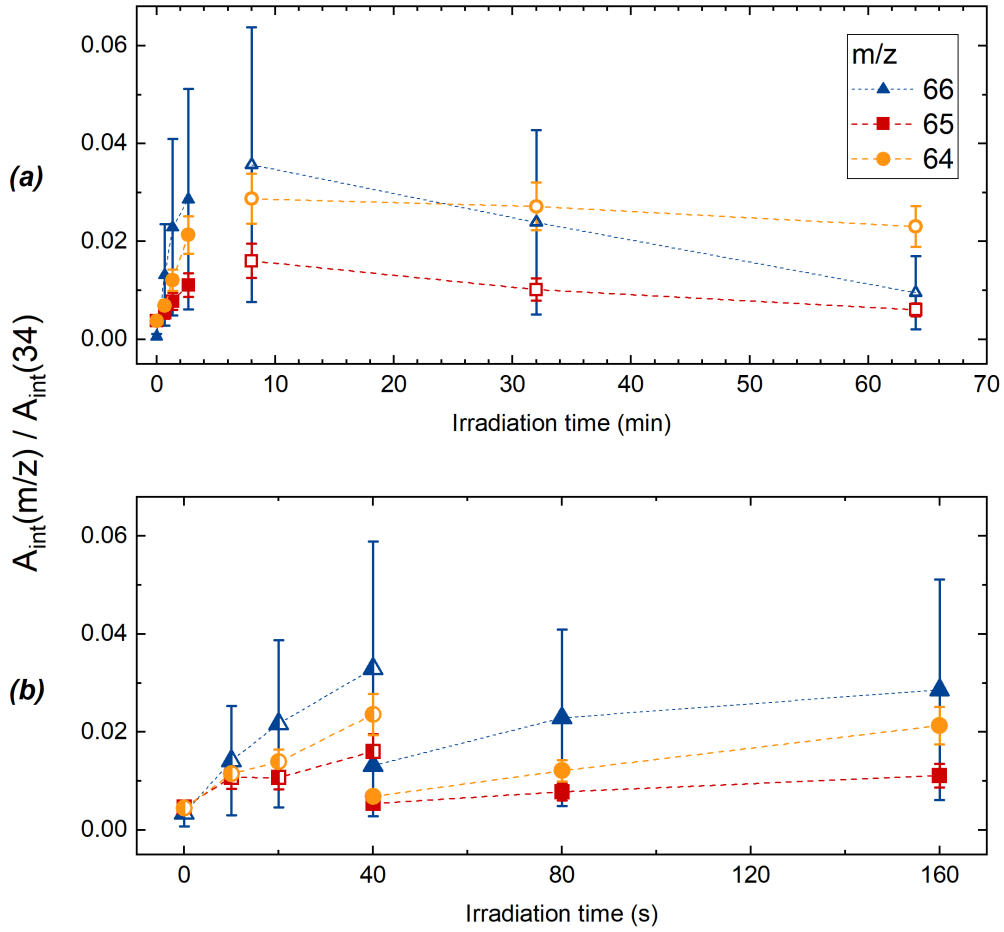

Figure 3.16: *Signal intensities of H_2S_2 fragments during irradiation relative to the main 34 m/z peak before irradiation using 70 eV ionization. The uncertainties are due to initial peak area spread (see text) and uniformity uncertainties.* `(a)` *Peak intensities for short irradiation periods. The solid (KIN-medium) and half-filled (KIN-short) markers represent two different experiments.* `(b)` *Peak intensities for longer irradiation periods. The solid markers are the same as the solid marker of the left panel. The solid (KIN-medium) and open (KIN-long) markers represent two different experiments.*

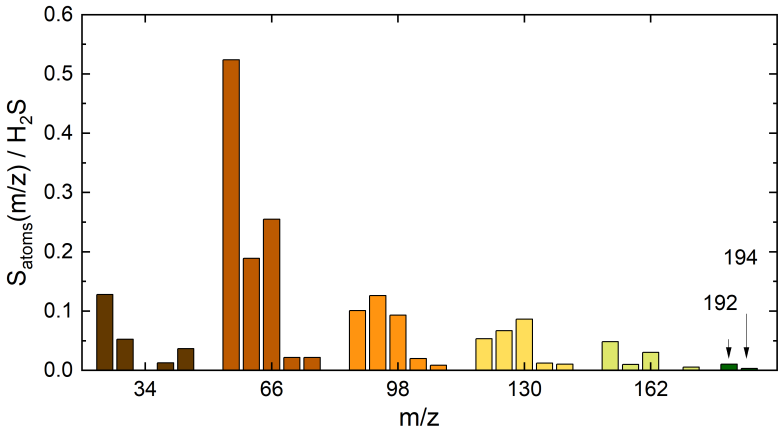

Figure 3.17: *Sulfur atom contributions to the sulfur budget compared to a single H_2S molecule after irradiation. In total there are 1.9 sulfur atoms for every H_2S molecule in an ice that has been irradiated for 64 minutes.*

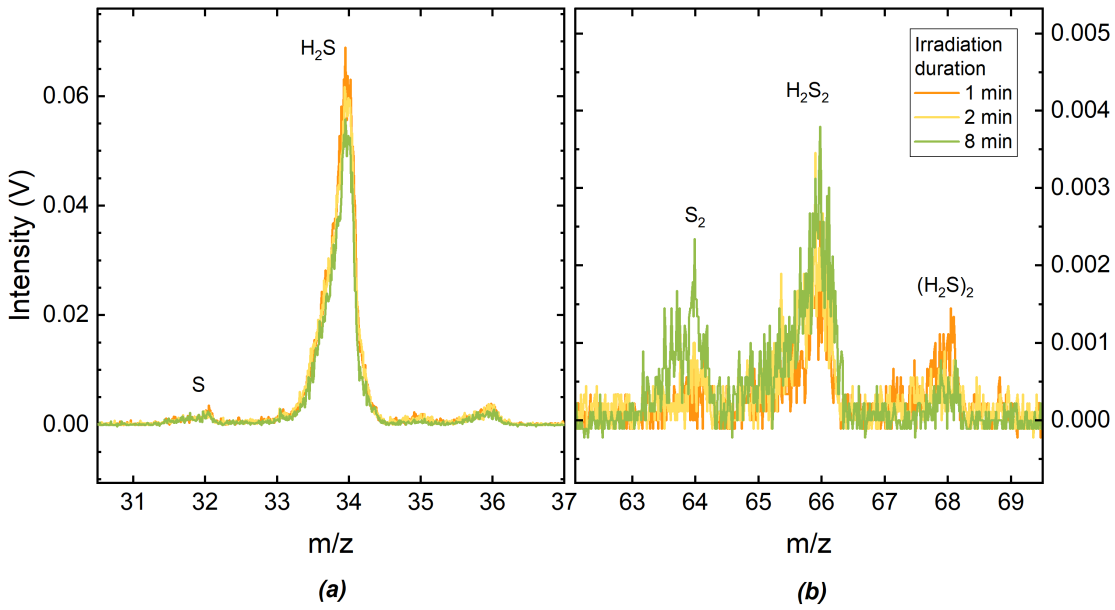

Figure 3.18: *Mass spectrum of H_2S ice during irradiation using 20 eV ionization. Note the change from teh 70 eV mass spectrum. (a) H_2S fragments. (b) H_2S_2 fragment with a likely cluster of H_2S.*

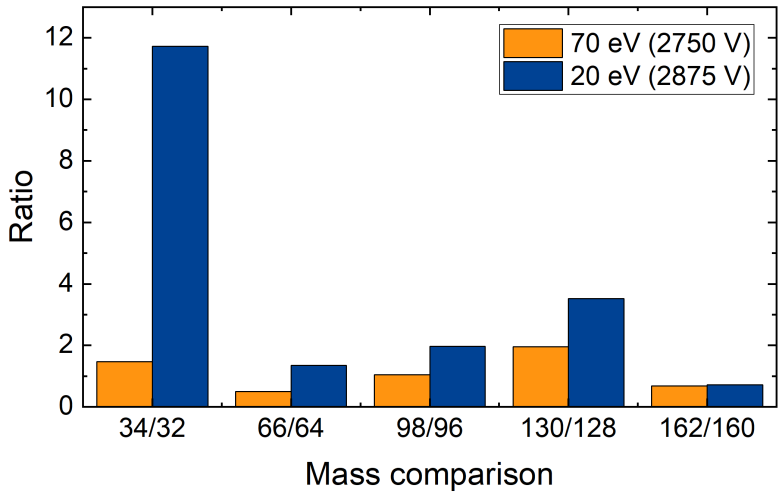

Figure 3.19: *Measured ratio between hydrogenated (H_2S_x) and unhydrogenated (S_x) sulfur products measured using 20 eV and 70 eV ionization.*

are stronger than their hydrogenated counterparts.
More measurements were taken at five temperatures between 15 K and 275 K. Figure 3.21 shows the relative decrease for hydrogenated sulfur chains as a function of temperature. The derived desorption temperature for each H_2S_x species are in good agreement with the value obtained from CRYOPAD2.

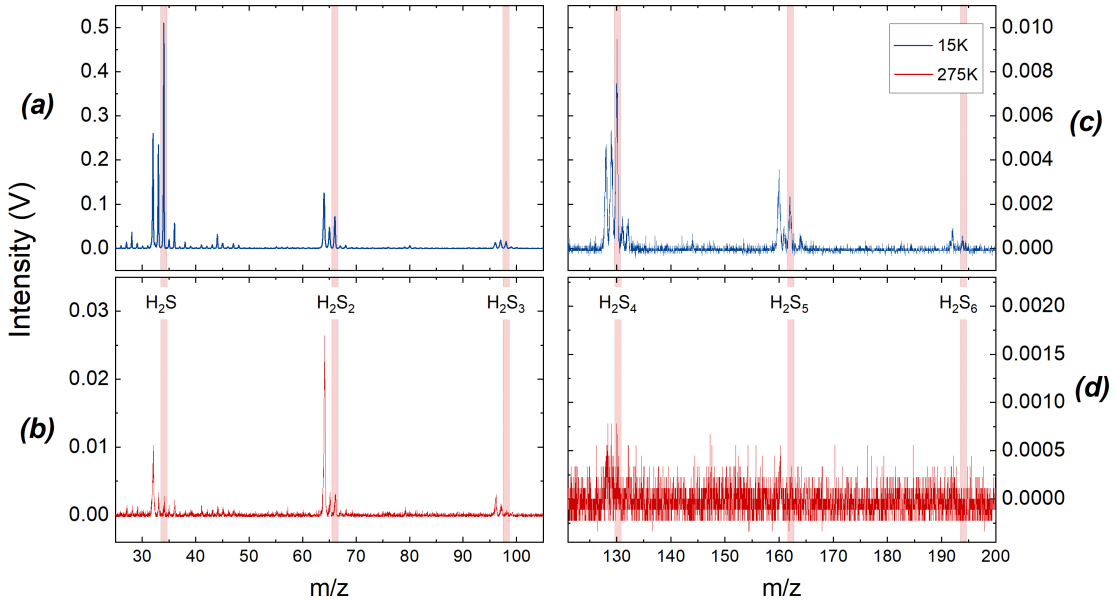

Figure 3.20: *Comparison between the mass spectra of the same irradiated H_2S which was irradiated at 15K and then measured at 15 K and 275 K. Both spectra were taken with the same MCP voltage (2775 V). The shaded areas correspond to the molecular ion mass of the labeled product.* `(a)`, `(c)` *Mass spectra at 15 K, hydrogenated peaks are still prominent.* `(b)`, `(d)` *Mass spectra at 275 K showing mostly unhydrogenated peaks.*

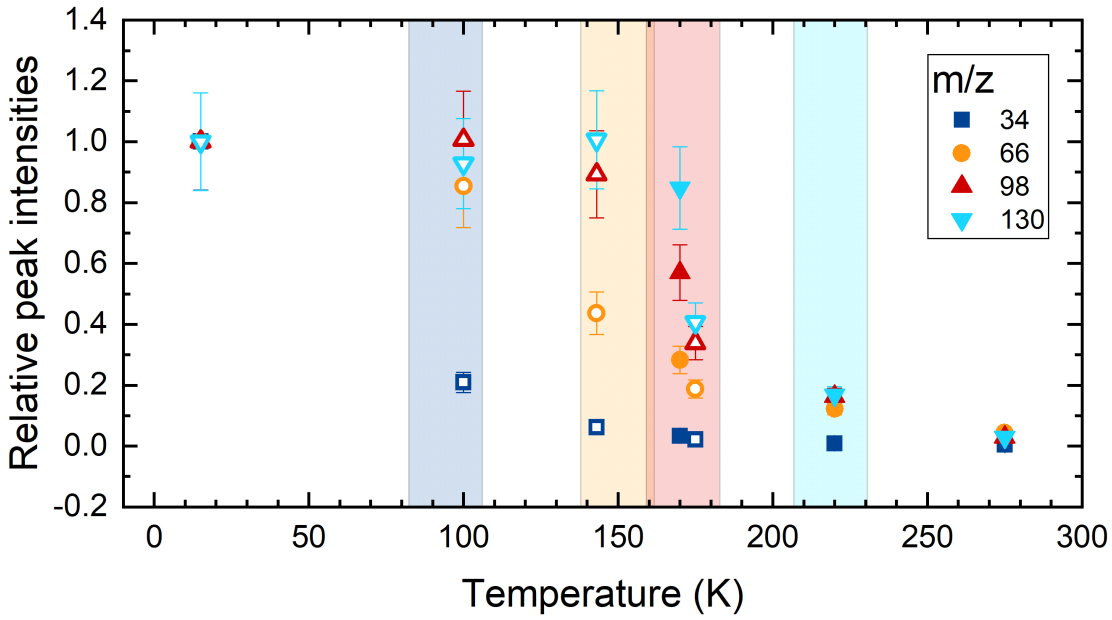

Figure 3.21: *The change in relative peak intensities (areas) is shown for mass spectra taken at different temperatures. The solid and open markers represent two different experiments. The peak intensities for both experiments were normalized so that the 15 K peak has a strength of 1. The colored shaded areas correspond to the desorption temperatures determined using CRYOPAD2: 85 K, 142 K, 165 K and 215 K.*

Chapter 4

Discussion

The aim of this bachelor research project is to study the photoproducts of irradiated H_2S ice in order to determine whether missing sulfur could be hidden in photoprocessed ices. We have compared the number of sulfur atoms stored in photoproducts compared to leftover H_2S after irradiation with 10^{18} photons cm^{-2} and found a lower limit of the relative abundance (S_{prod} / H_2S) to be 1.9. This means that the total sulfur budget (H_2S + S_{prod}) in the ice is a factor of 2.9 higher than the leftover H_2S. Subsequently, the total sulfur abundance is a factor 2.9 higher than detected H_2S. Limited mass range and worse mass sensitivity at higher masses mean that the actual sulfur budget could be higher. Additionally, we assume all H_2S is merely product even though H_2S_2 has a significant 34 m/z fragment (Julia de Carvalho Santos, private communication). These results cannot be directly applied to observations as the pure laboratory ices are unrepresentative of interstellar ices. The bulk of interstellar ice composition is H_2O followed by simple carbon-bearing compounds like CO, CO_2 and CH_3OH[6]. H_2S makes up only a small fraction of these ices. UV irradiation experiments with H_2S:CO and H_2S:CH_3OH mixtures have demonstrated the formation of OCS and CS_2[24]. Therefore the studied sulfur photochemistry with pure H_2S ice serves as a base to access the maximum yield of (hydrogenated) sulfur chains.

None of the photoproducts studied here have been directly observed in interstellar ices, so it is difficult to provide one to one comparison between laboratory and observational results. However, H_2S_2 was detected in the coma of 67P/Churyumov-Gerasimenko by the *Rosetta* space probe. H_2S_2/H_2S was measured to be 5.7×10^{-4} with an uncertainty of a factor of 10[10]. This is two orders of magnitude lower than our measured H_2S_2/H_2S ratio of 0.5 ± 0.1 after 1.1×10^{17} photons cm^{-2}. It is mostly likely because cometary ice is enriched in H_2O, significantly decreasing the possibility of SH radical recombination.

Assuming a flux of 10^4 photons cm^{-2}[25], the fluence received by the laboratory ices corresponds to 10^4 to 10^5 years which is within a dense molecular cloud's lifetime[24].

TPD experiments confirm desorption temperatures for the four smallest hydrogenated sulfur chains: 85 K (H_2S), 142 K (H_2S_2), 165 K (H_2S_3) and 215 K (H_2S_4). The desorption peak observed at 265 K (including masses of S_x, $2 \leq x \leq 5$) is likely due to H_2S_5 fragments. A linear correlation between the desorption temperatures of these hydrogenated sulfur chains and the number of containing sulfur atoms is found, giving high confidence in these values. The desorption temperatures for H_2S, H_2S_2 and H_2S_4 agree closely with results from Cazaux et al.[12], but the reported value for H_2S_3 is lower than the value reported in their work. This discrepancy may arise from different ice thicknesses as this can an effect on the desorption temperature[26]. No separate S_x peaks have been observed. Mass spectra taken at 275 K of irradiated H_2S ice show that smaller H_2S_x products have desorbed, but corresponding S_x peaks are still present. These are likely fragments of larger products, but the diminishing sensitivity at larger masses prevents the fitting of mass spectra for confirmation.
Experiments with 20 eV ionization have shown significant decrease in fragmentation for H_2S. If all products cease to fragment during ionization, it is unlikely that mass spectra will contain any HS_x signal since this is a radical and should fully hydrogenate. However, the mass resolution at 20 eV is too small to distinguish differences of 1 m/z, likely due to uncalibrated ion optics whose settings do not necessarily transfer from 70 eV to 20 eV. A more dedicated calibration is necessary to derive the quantitative results.

UV photons can penetrate through, and be absorbed by, the ice resulting in photodissociation of ice being a bulk process. The penetrating depth depends the total quantity of ice and is expressed by Beer-Lambert law. The photodissociation is a first-order reaction. Therefore, the depletion of ice follows an exponential decay. However, kinetic analysis of ice abundance during irradiation shows that it must be fit with a combination of exponential and linear components:

$$y = A \cdot \exp\{-\sigma x\} + b \cdot x + c \tag{4.1}$$

σ is the photodissociation cross section and b the linear desorption term, c and A are scaling terms and x denotes the H_2S (relative) column density. The linear desorption term derived from IR data results in rate of $(3.4 \pm 0.2) \times 10^{-2}$ molecules $photon^{-1}$, , which is about ten times higher than the desorption rate directly measured by QMS. The former value is obtained through a deconvolution resulting in the best fitting results. It is important to note that the fit is not a unique solution but acts as a base to understand the complex kinetic

evolution with a linear-exponential combination. The similar discrepancy is also found in analyzing CH_3OH photodesorption rate between IR and QMS data[27][28]. If we scale the initial quantity of H_2S in the irradiation experiments on MATRI^{2}CES (Figure 3.15) to the same initial H_2S column density as Exp. 1 (Figure 3.6), we calculate a desorption rate of 8×10^{-3}, which is in the same order of magnitude as the derived desorption rate using QMS. Photodissociation cross sections derived using TOF-MS and IR spectroscopy, $(9 \pm 4) \times 10^{-17}$ and $((9.3 \pm 0.5) \times 10^{-17})$, respectively, agree with one another.
In both experiments the quantity of H_2S_2 reached its maximum within a few minutes and did not increase further. TOF-MS has shown that H_2S_2 starts decreasing after receiving an irradiation dose of 1.5×10^{17} photons cm^{-2} (5×10^4 years in a dense molecular cloud).

Finally, we suggest two improvements of the MATRI^{2}CES setup for future ice irradiation studies. First of all, the mass range of TOF-MS should be increased in order to verify the formation of S_8, a speculated molecular carrier of the missing sulfur. Secondly, the sensitivity can be greatly increased using the second pulser; an electronic plate that deflects ions in a specific mass range. Thanks to the exclusion of overabundant species signal, the applied MCP voltage can be increased to obtain a higher detection sensitivity.

To summarize: this bachelor research project thoroughly studied the product formation during UV-irradiation of H_2S. Ices were analyzed using surface IR spectroscopy, quadrupole mass spectrometry and highly sensitive time-of-flight mass spectrometry. We conclude the following:

1. The total sulfur budget in irradiated H_2S ice is a factor of 2.9 higher than the unprocessed H_2S after receiving a UV fluence likely representative of dense molecular clouds.

2. The UV desorption rate of H_2S is determined to be $(3.3 \pm 0.3) \times 10^{-3}$ molecules photon^{-1}.

3. Experimental data do not provide evidence for the formation of pure sulfur allotropes as no corresponding desorption signals were found below 300 K while hydrogenated sulfur chains (H_2S_x, x up to 6) are dominant sulfur-bearing products.

Version of June 22, 2023– Created June 22, 2023 - 08:12

Chapter 5

Acknowledgements

Of course, a bachelor research project is anything but a solitary task. During the four months I got to work on this project, I have received immense help from everyone involved with the Laboratory for Astrophysics at Leiden University. I would like to begin by thanking Harold Linnartz, without whom this project would not have been possible and Tjerk Oosterkamp who has grasciously agreed to be my second reader. I hope there has been at least one thing in this thesis you will remember.
I am extremely grateful to Ko-Ju Chuang for showing me the ropes and being a constant support for the whole duration of the project. This thesis would not have existed without your advise and suggestions as I would have been overwhelmed a long time ago. Special thanks to Pranjal Samarth who taught me everything there is to know about MATRI^{2}CES and has been a wonderful mentor. I wish you all the best for the remaining two years of your PhD.
I'd like to thank everyone else for aiding me in my confusion and providing great company: Anita, Jeroen, Jerry, Julia and Katie. The science was good and so were the borrels. Finally want to thank Bryce and Charlotte for the amazing *herres energy* of these last four months.

Bibliography

[1] Hily-Blant, P., Pineau des Forêts, G., Faure, A., and Lique, F., *Sulfur gas-phase abundance in dense cores*, A&A **658**, A168 (2022).

[2] Martín-Doménech, R., Jiménez-Serra, I., Muñoz Caro, G. M., Müller, H. S. P., Occhiogrosso, A., Testi, L., Woods, P. M., and Viti, S., *The sulfur depletion problem: upper limits on the H2S2, HS· 2, andS2gas − phaseabundancestowardthelow − masswarmcoreIRAS*16293 − 2422, *A*&*A***585**, *A*112(2016).

[3] T. P. Snow and A. N. Witt, *Interstellar Depletions Updated: Where All the Atoms Went*, **468**, L65 (1996).

[4] M. Kama, O. Shorttle, A. S. Jermyn, C. P. Folsom, K. Furuya, E. A. Bergin, C. Walsh, and L. Keller, *Abundant Refractory Sulfur in Protoplanetary Disks*, The Astrophysical Journal **885**, 114 (2019).

[5] Marseille, M. G. and Cazaux, S., *The snow border*, A&A **532**, A60 (2011).

[6] M. K. McClure et al., *An Ice Age JWST inventory of dense molecular cloud ices*, Nature Astronomy **7**, 431 (2023).

[7] Jiménez-Escobar, A. and Muñoz Caro, G. M., *Sulfur depletion in dense clouds and circumstellar regions - I. H2S ice abundance and UV-photochemical reactions in the H2O-matrix*, A&A **536**, A91 (2011).

[8] A. C. A. Boogert, W. A. Schutte, F. P. Helmich, A. G. G. M. Tielens, and D. H. Wooden, *Infrared observations and laboratory simulations of interstellar CH_4_ and SO_2_.*, **317**, 929 (1997).

[9] M. E. Palumbo, T. R. Geballe, and A. G. G. M. Tielens, *Solid Carbonyl Sulfide (OCS) in Dense Molecular Clouds*, **479**, 839 (1997).

[10] U. Calmonte, K. Altwegg, H. Balsiger, J. J. Berthelier, A. Bieler, G. Cessateur, F. Dhooghe, E. F. van Dishoeck, B. Fiethe, S. A. Fuselier, S. Gasc, T. I. Gombosi, M. Hassig, L. Le Roy, M. Rubin, T. Semon, C.-Y. Tzou, and S. F. Wampfler, *Sulphur-bearing species in the coma of comet 67P/Churyumovâ€“Gerasimenko*, Monthly Notices of the Royal Astronomical Society **462**, S253 (2016).

[11] Y. Oba, T. Tomaru, T. Lamberts, A. Kouchi, and N. Watanabe, *An infrared measurement of chemical desorption from interstellar ice analogues*, Nature Astronomy **2**, 228 (2018).

[12] Cazaux, S., Carrascosa, H., Muñoz Caro, G. M., Caselli, P., Fuente, A., Navarro-Almaida, D., and Riviére-Marichalar, P., *Photoprocessing of H2S on dust grains - Building S chains in translucent clouds and comets*, A&A **657**, A100 (2022).

[13] C. N. Shingledecker, T. Lamberts, J. C. Laas, A. Vasyunin, E. Herbst, J. Kastner, and P. Caselli, *Efficient Production of S8 in Interstellar Ices: The Effects of Cosmic-Ray-driven Radiation Chemistry and Nondiffusive Bulk Reactions*, The Astrophysical Journal **888**, 52 (2020).

[14] J. Terwisscha van Scheltinga, *Ice and gas in protostellar clouds and planet-forming disks: a combined laboratory and observational study*, PhD thesis, University of Leiden, Netherlands, 2021.

[15] N. F. W. Ligterink, *The astrochemical factory: A solid base for interstellar reactions*, PhD thesis, University of Leiden, Netherlands, 2017.

[16] B. Teolis, M. Loeffler, U. Raut, M. Famá, and R. Baragiola, *Infrared reflectance spectroscopy on thin films: Interference effects*, Icarus **190**, 274 (2007).

[17] M. Bouilloud, N. Fray, Y. Bénilan, H. Cottin, M.-C. Gazeau, and A. Jolly, *Bibliographic review and new measurements of the infrared band strengths of pure molecules at 25 K: H2O, CO2, CO, CH4, NH3, CH3OH, HCOOH and H2CO*, Monthly Notices of the Royal Astronomical Society **451**, 2145 (2015).

[18] Y. Y. Yarnall and R. L. Hudson, *A New Method for Measuring Infrared Band Strengths in H2O Ices: First Results for OCS, H2S, and SO2*, The Astrophysical Journal Letters **931**, L4 (2022).

[19] M. Bulak, *UV Photodesorption and Photoconversion of Interstellar Ices - the laboratory perspective*, PhD thesis, University of Leiden, Netherlands, 2021.

[20] M. Berglund and M. E. Wieser, *Isotopic compositions of the elements 2009 (IUPAC Technical Report)*, Pure and Applied Chemistry **83**, 397 (2011).

[21] Muñoz Caro, G. M., Chen, Y.-J., Aparicio, S., Jiménez-Escobar, A., Rosu-Finsen, A., Lasne, J., and McCoustra, M. R. S., *Photodesorption and physical properties of CO ice as a function of temperature*, A&A **589**, A19 (2016).

[22] J. E. Hudson, C. Vallance, and P. W. Harland, *Absolute electron impact ionization cross-sections for CO, CO2, OCS and CS2*, Journal of Physics B: Atomic, Molecular and Optical Physics **37**, 445 (2003).

[23] M. Vinodkumar, H. Bhutadia, C. Limbachiya, and K. Joshipura, *Electron impact total ionization cross sections for H2S, PH3, HCHO and HCOOH*, International Journal of Mass Spectrometry **308**, 35 (2011).

[24] A. Jiménez-Escobar, G. M. Muñoz Caro, and Y.-J. Chen, *Sulphur depletion in dense clouds and circumstellar regions. Organic products made from UV photoprocessing of realistic ice analogs containing H2S*, Monthly Notices of the Royal Astronomical Society **443**, 343 (2014).

[25] Shen, C. J., Greenberg, J. M., Schutte, W. A., and van Dishoeck, E. F., *Cosmic ray induced explosive chemical desorption in dense clouds*, A&A **415**, 203 (2004).

[26] A. Jiménez-Escobar, G. M. M. Caro, A. Ciaravella, C. Cecchi-Pestellini, R. Candia, and G. Micela, *SOFT X-RAY IRRADIATION OF H2S ICE AND THE PRESENCE OF S2 IN COMETS*, The Astrophysical Journal Letters **751**, L40 (2012).

[27] Öberg, K. I., Garrod, R. T., van Dishoeck, E. F., and Linnartz, H., *Formation rates of complex organics in UV irradiated CH3OH-rich ices* - I. Experiments*, A&A **504**, 891 (2009).

[28] M. Bertin, C. Romanzin, M. Doronin, L. Philippe, P. Jeseck, N. Ligterink, H. Linnartz, X. Michaut, and J.-H. Fillion, *UV PHOTODESORPTION OF METHANOL IN PURE AND CO-RICH ICES: DESORPTION RATES OF THE INTACT MOLECULE AND OF THE PHOTOFRAGMENTS*, The Astrophysical Journal Letters **817**, L12 (2016).

Chapter 6

Appendix

During this four-month long project, we had the opportunity to explore various avenues which did not necessarily lead to conclusive results or were deemed not relevant for this thesis. In this chapter, these efforts are briefly discussed.

6.1 CRYOPAD2: H_2S irradiation with an argon cap

In order to more accurately identify photoproducts, a higher formation yield is profitable. For this reason we attempted to reduce the the desorption rate of H_2S as this would increase H_2S available for photoconversion. An argon cap (ice) was placed on top of the H_2S before irradiation in order to block desorption. Previous experiments have shown that this method indeed reduces desorption as a thicker argon cap lead to a smaller QMS signal.
An argon cap was deposited upon a 15 ML thick H_2S ice and irradiated after which a TPD was performed. During irradiation a desorption signal could be seen in the QMS. The desorption rate was a factor 2 lower than the uncapped (pure H_2S) ice as shown in Figure 6.1. Fitting an exponential-linear fit (as discussed in the paper) to the IR data showed a two order of magnitude decrease in the linear desorption term and an order of magnitude increase in the photodissociation cross section compared to the uncapped experiment (Figure 6.2.

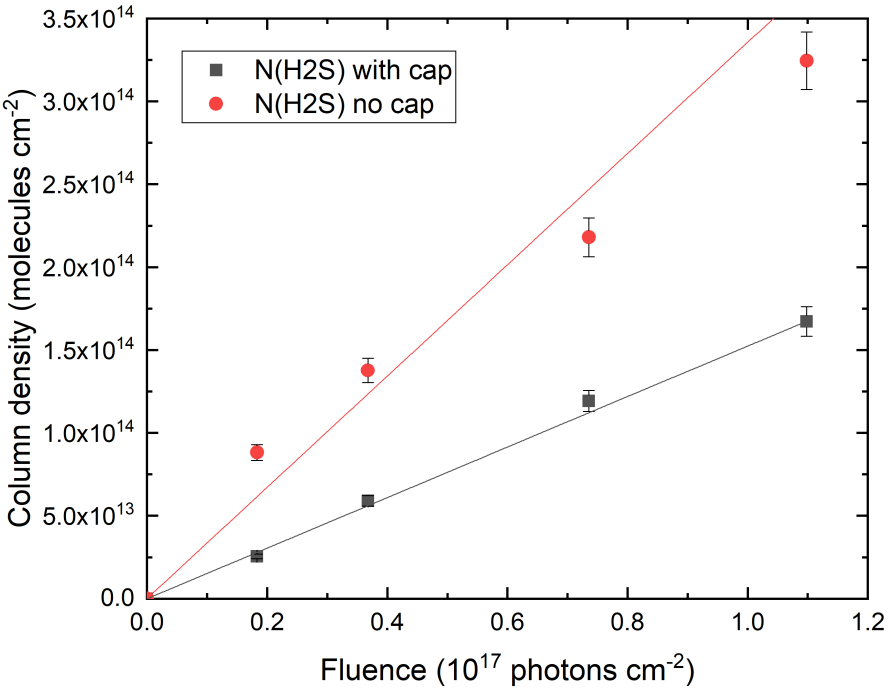

Figure 6.1: *Desorbed H_2S column density based on QMS data.*

6.2 MATRI^{2}CES

6.2.1 HOPG substrate

During the four months of this project half of the substrate on MATRI^{2}CES was covered in gold which reduced the number of available columns from 9 to 4. Since all ices were grown on both sides of the substrate, all experiments were performed on the HOPG (highly oriented pyrolytic graphite) side as well. These results were not mentioned in the main thesis as it is not relevant to the research question. The main effects of HOPG on H_2S was a higher photoproduct yield in general and a larger S_x/H_2S_x ratio (see Figure 6.3). Experiments with other ices (methanol, ammonia, water) showed that the carbon in HOPG tends to react with the ices under UV and form new products. Pure H_2S experiments showed the possible formation of ethene, likely due to the reaction between carbon and the hydrogen released during photodissociation of H_2S.

6.2.2 35 eV ionization

Since the 20 eV ionization experimetns did not yield significant results due to low mass resolution, ionization at 35 eV was attempted. It was hypothesized

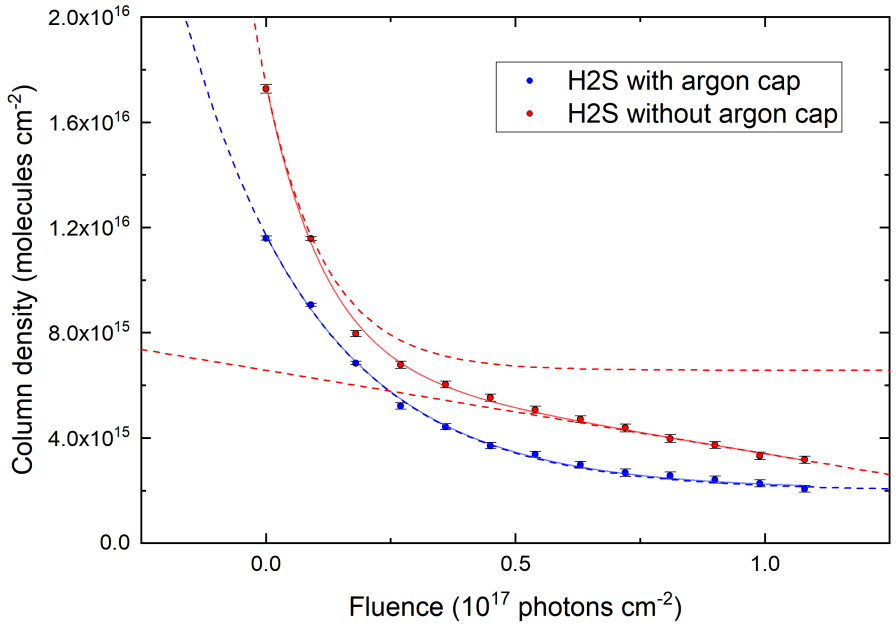

Figure 6.2: *Column densities of the capped and uncapped experiments (argon cap). The fit is a combination of a linear and an exponential function. the dashed lines represent the two terms separately. For the capped experiment, the data is almost perfectly described using a simple exponential term with a negligible linear term (which is not shown).*

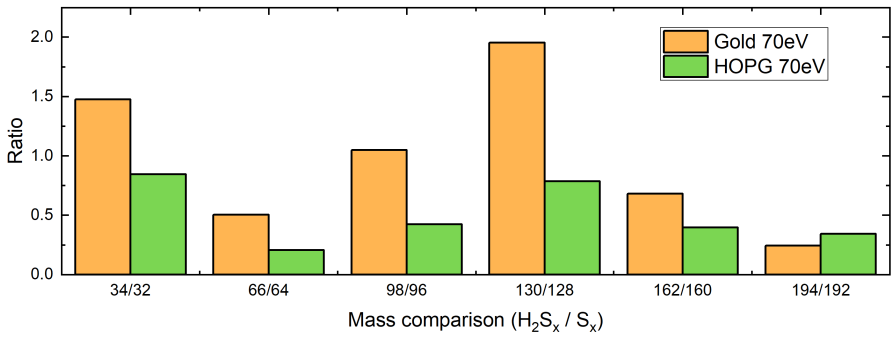

Figure 6.3: *Comparison of product formation on gold and HOPG after 64 minutes of irradiation. The ratio of hydrogenated (H_2S_x) to pure (S_x) sulfur products is shown as for different masses. HOPG shows more pure sulfur chains than gold.*

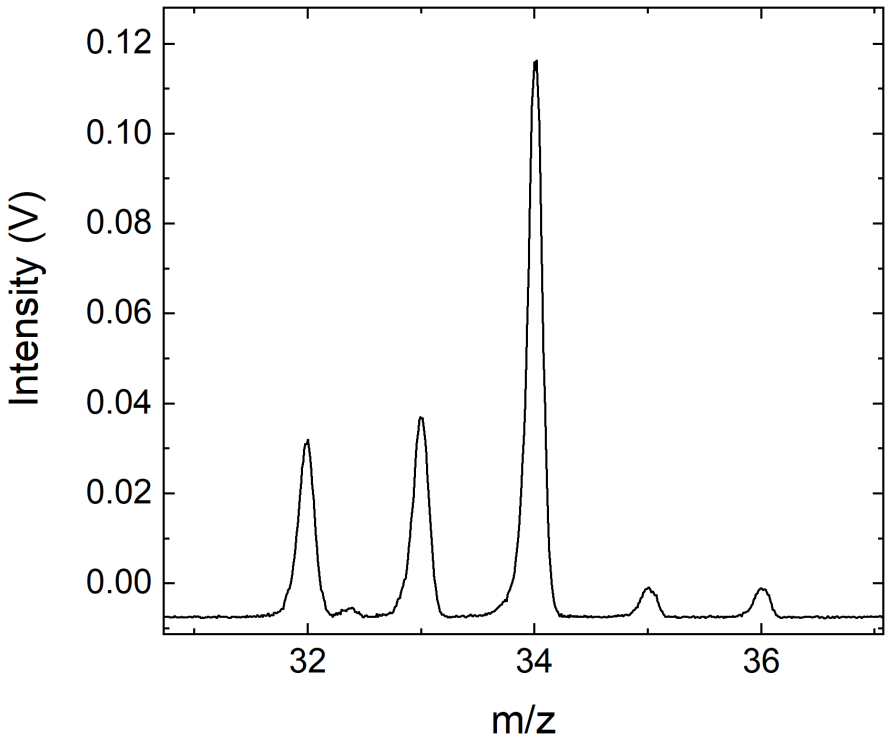

Figure 6.4: *H_2S fragmentation pattern at 35 eV.*

that this slight increase in ionization would increase mass resolution without significantly fragmenting the products. No previous experiments had been performed on MATRCI^{2}CES at 35 eV, so the focus energy (F.E.) of the electron gun had to be optimized. The optimal F.E. was determined to be 19 eV. Mass spectra at 35 eV revealed the fragmentation pattern of H_2S to be almost identical to the pattern at 70 eV, as shown in Figure 6.4, so no further experiments were performed.

6.3 SURFERSIDE irradiation and TPD

Since no further experiments could be performed on CRYOPAD2, as it had been refurbished for another project, an irradiation and TPD experiment (same procedure as Experiment 1) was performed on the SURFERSIDE setup in the Laboratory for Astrophysics at Leiden University. This setup has all capabilities of the CRYOPAD2 setup, but possesses a less sensitive QMS. During the heating process, only a few masses could be observed (32 m/z, 34 m/z, 64 m/z and 66 m/z). The H_2S and H_2S_2 desorption temperatures agree with CRYPAD2 data.